# Linear and Nonlinear Convection in Porous Media between Coaxial Cylinders

Master of Science Thesis in Applied and Computational Mathematics

Carina Bringedal

Department of Mathematics
University of Bergen


May 2, 2011

# Acknowledgements

First of all I would like to thank my supervisors Inga Berre and Jan M. Nordbotten for all their help, good discussions and useful feedback. Their enthusiasm and support have made this process easier and more cheerful. Also I would like to thank Professor D. Andrew S. Rees for helping me getting a better understanding of the convection cells, for valuable help concerning the analysis and interpretation of results, and for taking the time to visit me in Bergen.

I thank my fellow students for making the days at the Math department happier and more interesting. Good luck with your bachelor/master/Ph.D. degrees! To my friends, thank you for getting me away from the University from time to time. I especially thank Line for always being there.

Finally, thank you Monica for helping me realize there are more important things in life than a master thesis.

*Carina,*
*April 2011.*

# Abstract

In this thesis we develop a mathematical model for describing three-dimensional natural convection in porous media filling a vertical annular cylinder. We apply a linear stability analysis to determine the onset of convection and the preferred convective mode when the annular cylinder is subject to two different types of boundary conditions: heat insulated sidewalls and heat conducting sidewalls. The case of an annular cylinder with insulated sidewalls has been investigated earlier, but our results reveal more details than previously found. We also investigate the case of the radius of the inner cylinder approaching zero and the results are compared with previous work for non-annular cylinders.

Using pseudospectral methods we have built a high-order numerical simulator to uncover the nonlinear regime of the convection cells. We study onset and geometry of convection modes, and look at the stability of the modes with respect to different types of perturbations. Also, we examine how variations in the Rayleigh number affects the convection modes and their stability regimes. We uncover an increased complexity regarding which modes that are obtained and we are able to identify stable secondary and mixed modes. We find the different convective modes to have overlapping stability regions depending on the Rayleigh number.

The motivation for studying natural convection in porous media is related to geothermal energy extraction and we attempt to determine the effect of convection cells in a geothermal heat reservoir. However, limitations in the simulator do not allow us to make any conclusions on this matter.

# Contents

# Outline and Motivation

A growing world population and an overall increase of wealth and welfare demands a large increase in the energy supply. Stable, long term solutions are needed in order to ensure the world's needs, and increased extraction of geothermal energy is a natural alternative. Geothermal energy is considered as a renewable energy resource, and is stable as it does not depend on weather conditions and is capable of producing energy with same effect all year long [28].

Several approaches for extracting geothermal energy exist, but the general idea is to pump cold water down a vertical well and receive hot water back. The obtained temperature difference generates an energy profit used for heating applications or to create electricity through a turbine. Understanding the heat transfer mechanisms in a geothermal system is essential in order to optimize the heat extraction and produce commercialy competitive electricity.

Natural convection represents an important process in geothermal systems. This thesis will present new insights in this phenomenon based on analytical and numerical studies of an idealized physical setting.

**In Chapter 1** we present the concept of geothermal energy and further motivate why geothermal energy extraction should be a part of satisfying the world's energy demands. We explain the different processes of heat transfer in porous media, with special focus on natural convection and the occurence of convection cells. In the end we explain why convection cells are of importance in geothermal energy extraction.

**In Chapter 2** we introduce basic definitions and concepts from reservoir engineering and fluid mechanics that are needed to develop a model for natural convection. Based on the governing physical laws concerning flow in porous media, we present the equations necessary in building a mathematical framework for describing the convection cells.

Flow and heat transfer in porous media is affected by various physical processes. Describing these processes to full detail for a real-world application, would be a task too comprehensive for the scope of this thesis. In order to obtain an increased understanding of the processes of natural convection, we consider a particular idealized, but relevant physical setting.

**In Chapter 3** we nondimensionalize the governing equations and also introduce suitable (nondimensional) boundary conditions. The dimensionless equations together with the boundary conditions constitute the mathematical model concerning the rest of the thesis.

**In Chapter 4** we apply a linear stability analysis to the mathematical model and obtain an analytical solution of the linearized equations through separation of variables. The analytical solution enables us to find critical Rayleigh numbers, which act like criterions for onset of natural convection. We also introduce the concept of convection modes, explain their geometrical structure and present a strategy of how to determine the preferred convective modes using the analytical solution.

**In Chapter 5** the results from the linear stability analysis are presented. Using the analytic framework developed in Chapter 4, we provide contour plots of the critical Rayleigh number and mode maps giving the convective mode as a function of the horizontal extent of the annular cylinder. We discuss the results and compare with previous papers on the subject.

**In Chapter 6** we introduce spectral methods, which are used to solve the governing nonlinear equations. Spectral methods are divided into Galerkin spectral methods and pseudospectral methods, and we present both classes of methods before we argue for the choice of pseudospectral methods. We explain how the choice of collocation points affects the pseudospectral methods and describe the structure of a pseudospectral discretization for our choices of collocations points. We also give a short presentation of the time discretization and sketch the convergence properties of the pseudospectral methods.

**In Chapter 7** we present the results from the nonlinear regime obtained using the pseudospectral code designed in Chapter 6. We compare simulated results with results from the linear regime with respect to critical Rayleigh number and preferred convective mode. The stability of the convection cells when subject to different types of perturbations is also presented. At last we present some preliminary experiments concerning the effect of convection

cells on a geothermal reservoir with respect to heat extraction.

**In Chapter 8** a summary is given together with conclusions and remarks on further work.

The analysis made in Chapter 4 and the results presented in Chapter 5 and Sections 7.1 and 7.2 are based on a co-authored unpublished paper:
C. Bringedal, I. Berre, J. M. Nordbotten and D. A. S. Rees. Linear and nonlinear convection in porous media between coaxial cylinders. *Submitted to Physics of Fluids*, 2011.

My contribution to this paper was performing the linear analysis, developing and implementing the code for the nonlinear regime and carry out all simulations, as well as being the main contributor in the writing of the manuscript. Berre, Nordbotten and Rees provided ideas, suggestions and guidance along the way and helped me interpret the results.

# Chapter 1

# Geothermal Energy

Geothermal energy is the thermal energy stored in the Earth's crust. In this chapter we give a short introduction to geothermal energy extraction, explain what convection cells are, and why they can be important for extraction of geothermal energy.

## 1.1 Geothermal Energy Extraction

The following presentation is mainly based upon the 2006 MIT report about the future of geothermal energy [28] and the book about geothermal energy and the environment [16].

The temperature of the Earth's crust increases with depth, with a maximum at the Earth's centre. This heat is partly excess temperature after the creation of the Earth, and partly due to heat created through the decay of radioactive particles. Using the heat for either direct heating purposes or for electricity generation is today exploited to some extent, but the potential is far from reached.

There is a large variety in anthropogenic systems for extracting geothermal energy; including several injecting and producing wells, open or closed systems and fracturing of the ground. The obtainable effect from extracting geothermal energy at a specific location depends on several factors as the ground's permeability, porosity, heat conductivity, availability of ground water and local heat production, to mention some. But one of the most important factors is the vertical temperature gradient, also called the geothermal gradient. A large geothermal gradient means that the ground reaches higher temperatures at lower depths, which is an obvious advantage for the extrac-

tion of geothermal energy.

Today, most of the geothermal energy extraction takes place near edges of tectonic plates. At these locations, the geothermal gradient is significantly larger. Nevertheless, since the areas with large geothermal gradients are very limited, the main potential for geothermal energy extraction lies in the sum of all land area having significantly lower geothermal gradients. Being able to extract geothermal energy at economically feasible rates at these locations is therefore essential for the future of geothermal energy extraction.

The main advantage of geothermal energy extraction compared to other renewable energy resources, is the energy security: Geothermal energy can be produced continuously. Geothermal energy also has several environmental advantages, making it preferable over fossil energy resources.

Running a geothermal power plant will include some environmental impact mainly in terms of emission of greenhouse gases, use of fresh water and influence on the nearby land. The most common emissions of greenhouse gases from a geothermal installations are carbon dioxide ($CO_2$) and hydrogen sulfide ($H_2S$). The emissions are due to the gases being naturally present in the ground and hence released during drilling, and also during production in open systems. However, the geothermal plants emit much less greenhouse gases per produced megawatt-hour than fossil-fueled power plants. See the MIT-report [28], Chapter 8.1, for details.

Geothermal projects need fresh water in both the drilling and the production process. However, water is always recirculated after cooling, hence the need of supplying more fresh water is normally small. Closed systems will in practice have no water loss during production. For comparison, a geothermal plant uses on average 19 liters per megawatt hour of produced electricity, while a natural gas plants needs approximately 1 350 liters per megawatt hour.

A geothermal power plant needs far less land area for producing electricity compared to other energy resources. However, drilling geothermal wells may induce seismicity. During drilling in Basel, Switzerland, between Desember 2006 and March 2007, 10 500 seismic events, the largest up to 3.4 at the Richter Magnitude scale, were measured and linked to the geothermal project [10].

## 1.2 Heat Transfer in Porous Media

Heat transfer is the transition of thermal energy from warmer regions to cooler regions and occurs via conduction, convection, phase change and radiation [5]. In porous media heat transfer is primarily in the form of conduction and convection.

Conduction is the transfer of thermal energy between neighbouring molecules in a substance due to molecular vibrations and collisions. The energy is always transferred from regions with higher temperature towards regions with lower temperature at a rate proportional to the temperature gradient. Consequently heat conduction has a smoothening effect on the temperature field.

When the motion of the fluid assists heat transfer from a surface, the situation is called convection. The motion of molecules in fluids can be in the form of random diffusion or advection. Both diffusion and advection lead to mass transfer and heat transfer, but the term "convection" in the context of mass or heat transfer, refers to the sum of diffusive and advective transfer. Convective heat transfer is divided into forced and natural convection.

- Forced convection is a type of heat transfer in which external sources, such as a pump or a fan, generate fluid motion.
- Natural convection is a type of heat transfer in which expansion and buoyancy forces generate fluid motion. Density differences in the fluid, which are due to temperature gradients, causes these forces. Fluids that receive heat become less dense and rise. Cooler fluids that move to replace the heated fluids are then heated themselves and the process continues. The heat is transferred from bottom to top because of this motion in the fluid.

Mixed convection is when both forced and natural convection is present. Normally both conductive and convective heat transfer will occur in a medium, but often one will dominate the other. The relative size of conductive and convective heat transfer is important for characterizing the medium.

## 1.3 Convection Cells in Geothermal Energy Extraction

Convection cells is a phenomenom in fluid dynamics that occurs in situations where there are density differences in the fluid. If we initially have a stationary fluid where the density in some layer is greater than in an underlying one,

a small disturbance may cause the fluid to start flowing. This fluid flow is called convection currents, and the convection currents may form convection *cells* [3]. The process is similar to the one described for natural convection; the light, warmer fluids rise, while the heavy, cooler fluids sink. However, when talking about convection cells it is implied that the streamlines are closed, hence the fluid particles are following closed trajectories circulating in the (porous) medium. Natural convection can cause convection cells to occur, but convection cells may also be caused by forced and mixed convection.

The process in a convection cell is as following: we assume an initial state of a stationary fluid where the lower fluid is lighter than the above fluid, normally due to the density being dependent on temperature. Many fluids, such as water, are denser when cold. A porous medium with heating from below and cooling from above, will therefore posess this initial state. Then, due to a perturbation or disturbance, some of the warm, lighter fluid starts to rise. Under the right circumstances, the fluid will continue to rise and the rising fluid particles will be cooled by the colder surroundings and become denser. At some point the fluid becomes denser than the fluid underneath it, which is also rising, and moves to the side instead. After some time, the fluid particle's downward force overcomes the rising force beneath, and the fluid descends. As it descends, the fluid receives heat from the warmer surroundings, becoming lighter again. Once down where the fluid started out before the perturbation, the cycle repeats itself. Schematically, the convection cells may behave as sketched in Figure 1.1.

As mentioned earlier, when determining the location of a new geothermal plant, subsurface heat properties are highly important. A large geothermal gradient and large vertical heat flow are desirable. Convection cells initially present in the subsurface will locally increase (or decrease) the geothermal gradient: In the upflow part of a convection cell, hot fluid is brought closer to the surface, hence the geothermal gradient will be larger for the upper part of the cell. Similarly convection cells locally increase (or decrease) the vertical heat flow. Knowing the location of the initial convection cells is essential for the geothermal industry, and several surveys regarding mapping the geothermal gradients and vertical heat flow have been made: For example, Chapman and Rybach [8] points out that the high temperature gradients in Roosevelt Hot Springs and in Monroe are caused by natural convection, while several papers concerning the Rhine-Graben reveals convection cells affecting the geothermal gradients and the vertical heat flow [1, 9, 17].

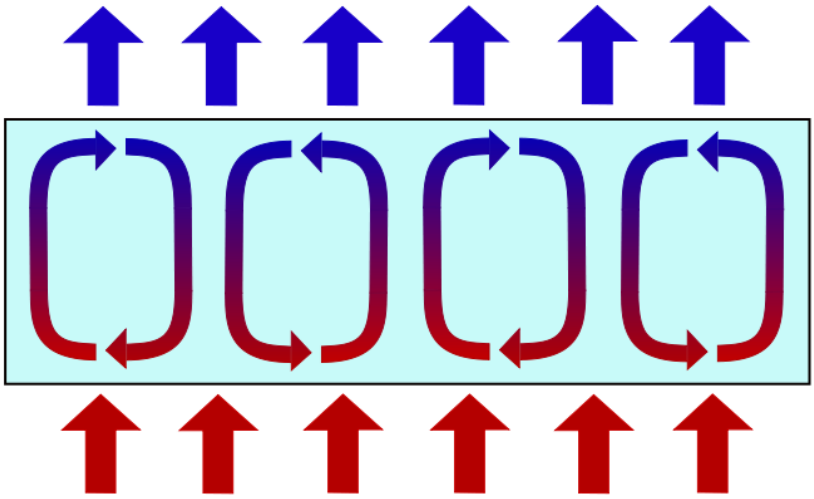

Figure 1.1: Convection currents in a porous medium which is heated from below and cooled from above.

Another possible advantage of convection cells in the context of geothermal energy extraction, is the cells' ability to retrieve heat far away from the geothermal well. If no convection is present in the system, all heat transfer occurs owing to conduction. In a convection dominated system, conduction will still contribute to the heat flow, but in addition the convective flow is able to retrieve heat far away from the well. The importance of this extra heat transfer depends on the horizontal extent and the velocity of the convection cells.

# Chapter 2

# Theory from Reservoir and Fluid Mechanics

We introduce basic definitions and concepts concerning flow in a porous medium in order to understand and describe the physics governing convection in porous media. Important definitions are given and basic equations used in reservoir engineering and fluid mechanics are presented. This will result in a framework making it possible to create a complete model of the convection cells in the next chapter. The following presentation is mainly based upon the books of Bear [3] and Nield and Bejan [21].

## 2.1 Porous Media

There are numerous examples of porous media: soil, porous rock, ceramics and bread are just a few. They all have in common that they may be described as "solids with holes". However, defining a porous medium as a solid with holes would not be a good definition since this would include a solid containing an isolated hole, which is normally not considered as a porous medium. We therefore demand the holes to be interconnected, allowing fluid transport through continuous paths from one side of the medium to another.

The pores form a complex structure within the medium, and in order to describe the pores mathematically, we consider the pore network as random variations having a well defined average. Therefore, quantities within a porous medium are considered as averages over a *representative elementary volume* (REV) [3]. An REV consists of the solid, which is normally a form of rock, and the void space in between the solid. This void space is randomly distributed, but is assumed to form an interconnected pore network allowing

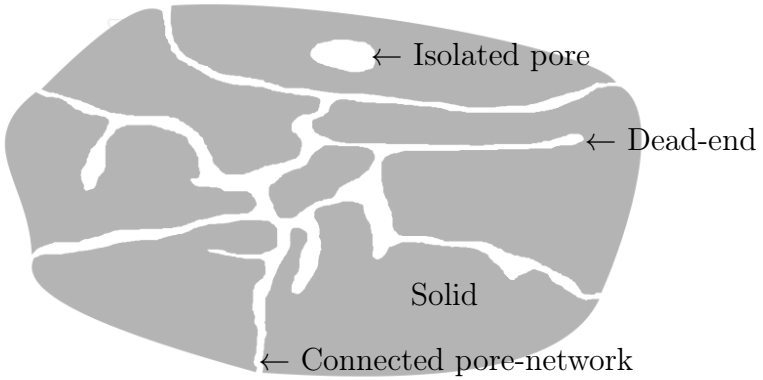


Figure 2.1: A porous medium with connected pores, isolated pores and dead-ends.

fluid flow as well as dead-ends and isolated pores, see Figure 2.1. We define the porosity $\phi$ of an REV as the ratio between the pore volume $V_P$ and the total volume $V_T$ within the REV, that is

$$\phi = \frac{V_P}{V_T}.$$

Since the dead-ends and isolated pores do not contribute to the fluid flow, only interconnected pores are of interest from the standpoint of flow through the porous medium. Hence we introduce the concept of *effetive* porosity $\phi_E$, defined as the ratio of the interconnected (or effective) pore volume $V_{EP}$ to the total volume of the REV;

$$\phi_E = \frac{V_{EP}}{V_T}.$$

As only the effetive porosity is used, we drop the word "effective" and the subscript $E$ when referring to effective porosity.

The porosity is a scalar quantity that may vary with position in the porous medium. A varying porosity will affect the flow in a porous medium, see for instance the paper of Vafai [30] which consideres the effect of varying porosity for convective flow and heat transfer. In this thesis only homogeneous porous media will be considered; we are not interested in the effect of a varying porosity, only in the convection cells themselves. Hence, the porosity will be assumed to be constant throughout the medium.

## 2.2 Fluid Properties

### 2.2.1 Density

Fluid density $\rho$ is defined as the mass of the fluid per unit volume and has SI-unit kg/m$^3$. In general density can vary with both pressure $P$ and the temperature $T$, and the relation between these three quantities is called an equation of state:

$$\rho = \rho(P, T).$$

We will assume the density to not depend on pressure, and vary linearly with temperature, that is

$$\rho = \rho_0[1 - \beta(T - T_0)], \tag{2.1}$$

where $\rho = \rho_0$ at some reference temperature $T_0$. The constant $\beta$ is called the thermal expansion coefficient. Since we will consider water, which becomes less dense for increasing temperatures, $\beta$ is a positive number.

We also apply the Boussinesq approximation, which states that small density differences can be neglected, except when they appear in terms multiplied by the gravity acceleration $g$. Together with the equation of state (2.1) this means that $\beta$ is a small number which is set to zero unless multiplied with $g$.

### 2.2.2 Viscosity

Fluids, unlike solids, will deform continuously when shear stress is applied. We refer to this continuous deformation as the fluid flow. Viscosity $\mu$ is a measure of the fluid's ability to resist deformation when in motion and has SI-unit kg/ms. A fluid with high viscosity may be thought of as being "thick", for example honey or heavy oil, while a fluid having low viscosity, such as water, is a "thin" fluid. Normally the viscosity of a fluid will depend on both temperature and pressure.

Both viscosity and the termal expansion coefficient may vary with temperature and pressure, but for simplicity we assume both to be constant. For an analysis of the effects when considering temperature dependent viscosity and thermal expansion coefficient, see the paper of Horne and O'Sullivan [14].

## 2.3 Permeability and Darcy's Law

For fluid flowing through a porous medium, Darcy's law is a phenomenological equation describing the flow. Henry Darcy experimented with water streaming through a horizontal layer of sand having length $L$, and by using different types of sand he discovered the relation

$$Q = \hat{K} A \frac{\Delta P}{L},$$

where $Q$ is the volume of flow per unit time, $\hat{K}$ is a proportionality constant, $A$ is the cross-sectional area of the layer and $\Delta P$ is the pressure drop over the sand sample.

The constant of proportionality, $\hat{K}$, is called the hydraulic conductivity and may be expressed as

$$\hat{K} = K \frac{\gamma}{\mu}$$

[3], where $K$ is the permeability of the porous matrix, and $\gamma/\mu$ represents the influence of the fluid's properties where $\gamma = \rho g$ is the specific weight of the fluid and $\mu$ is the viscosity of the fluid. The permeability of a porous medium is a measure of the medium's ability to transmit fluid, and a high permeability means that fluid easily can flow through the medium. The unit of permeability is Darcy, which converted to SI-units yields 1 Darcy $\approx 0.987 \cdot 10^{-12}\ m^2$.

In general, the permeability can depend on both spatial location and the direction of flow. When the permeability depends on location, we write $K = K(x, y, z)$ and the medium is heterogeneous. If the permeability depends on the direction of flow, $K$ can be expressed as a tensor $\mathbf{K}$, and we call the medium anisotropic. A lot of work has been done related to heat transfer in heterogeneous and anisotropic porous medium, see for instance Chapter 6.12 and 6.13 in [21] for an overall discussion around this matter. However, these concerns will not be a subject in this thesis. We will only consider a porous medium that is homogeneous and isotropic, hence the permeability is a constant scalar.

Allowing the fluid to flow in all directions, and writing the equation in differential form, yields the modern version of Darcy's law:

$$\mathbf{v} = -\frac{K}{\mu}(\nabla P + \rho g \mathbf{k}). \tag{2.2}$$

Gravity acceleration is denoted by $g$, and $\mathbf{k}$ is a vertical unit vector, pointing upwards. Furthermore, $\rho$ is the density of the fluid and $\mathbf{v}$ is the Darcy

velocity. Note that the Darcy velocity is not the actual velocity of the fluid particles inside the pores. If we average the fluid velocity over an REV, we get the intrinsic average velocity $\mathbf{V}$, which is related to the Darcy velocity through the Dupuit-Forchheimer relationship $\mathbf{v} = \phi\mathbf{V}$ [21].

Darcy's law is only valid for describing the fluid flow in a porous medium when the Darcy velocity is so small that friction between the flowing fluid and the pore walls are dominating the system. If the velocity is too large or the fluid too thin (that is, low viscosity) such that friction is no longer dominating, turbulence will arise causing Darcy's law to fail. Typical velocities for most cases concerning flow in porous medium is in the order of cm/hour or lower [22], which is in the scope of Darcy's law. Bächler, Kohl and Rybach [1] reported that the flow velocity for natural convection in Rhine-Graben is approximately $10^{-9}$ m/s $\approx$ 0.1 mm/day, hence it is reasonable to assume that our velocities will be in the same order of magnitude and Darcy's law is applicable. Darcy's law also requires only one fluid phase present in the porous medium: In this thesis we assume only water is saturating the porous medium[1]. The last requirements of Darcy's law are that the saturating fluid should not react physically or chemically with the medium, and are satisfied by assumption.

## 2.4 Mass Conservation

Conservation laws describes how an extensive property is conserved within a closed system. An extensive quantity depends on the size of the system or the amount of material in the closed system. For example is mass and energy extensive variables, while pressure and temperature are intensive variables. Both mass and energy are conserved within a closed system and we express this through conservation laws. To derive the mass conservation equation, we must account for the processes that influence mass.

We encounter a fixed geometric volume $\Omega$ having boundary $\partial\Omega$ and outward unit normal $\mathbf{n}$, see Figure 2.2. The volume consists of a solid with pores in which fluid may flow in, and we conserve the mass of the *fluid*. Fluid may leave or enter the volume $\Omega$ through the boundary, or it may be produced or

[1] Using supercritical $CO_2$ in stead of water as working fluid in geothermal energy extraction was suggested by Brown [7]. His conclusion is that supercritical $CO_2$ has favourable properties compared to water when used in a Hot Dry Rock (HDR) system. This has later been confirmed by theoretical and numerical studies [23, 24], but field experiments are not yet performed.

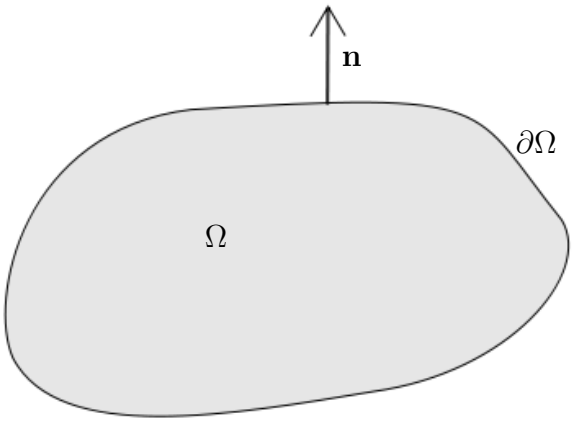


Figure 2.2: Fixed geometric volume $\Omega$ with boundary $\partial\Omega$ and outward normal unit $\mathbf{n}$.

annihilated in a source or sink. The accumulation of mass inside the volume has to equal the produced mass through sources minus the mass lost through sinks and minus the net rate of mass flowing out of the volume. This can be written

$$\{\text{Accumulation}\} + \{\text{Net Rate Flowing Out}\} = \{\text{Sources}\} - \{\text{Sinks}\}. \quad (2.3)$$

We assume there are no sources or sinks inside the volume. The accumulation of mass is given as the time derivative of the total mass, that is

$$\frac{d}{dt}\int_{\Omega} \phi\rho \mathrm{dV},$$

where $\phi$ is the porosity of the porous medium filling the volume and $\rho$ is the density of the saturating fluid. The integral expresses the total mass of fluid inside the pores of the volume. The net volume of fluid flowing out through the boundary of the volume is given as

$$\int_{\partial\Omega} \rho\mathbf{v}\cdot\mathbf{n}\mathrm{dS},$$

where $\mathbf{v}$ is the Darcy velocity and $\mathbf{n}$ is the outward unit normal as observed in Figure 2.2. We insert these expressions into the conservation law (2.3) and obtain

$$\frac{d}{dt}\int_{\Omega} \phi\rho \mathrm{dV} + \int_{\partial\Omega} \rho\mathbf{v}\cdot\mathbf{n}\mathrm{dS} = 0.$$

We apply Leibniz integral rule,

$$\frac{d}{dt}\int_{\Omega} f(x,t)\mathrm{dV} = \int_{\Omega}\frac{\partial f}{\partial t}\mathrm{dV},$$

to the first term, and Gauss theorem,

$$\int_{\partial\Omega}\mathbf{F}\cdot\mathbf{n}\mathrm{dS} = \int_{\Omega}\nabla\cdot\mathbf{F}\mathrm{dV},$$

to the second term. Since our volume $\Omega$ is arbitrarily chosen and the integrand continuous, we obtain the pointwise mass conservation equation for flow in a porous medium,

$$\phi\frac{\partial\rho}{\partial t} + \nabla\cdot(\rho\mathbf{v}) = 0.$$

Recall that the Boussinesq approximation introduced earlier allows us to neglect all density differences unless they appear in terms multiplied with the gravity acceleration. Owing to this approximation we can remove the time derivative of the density, and the mass conservation equation becomes

$$\nabla\cdot\mathbf{v} = 0. \tag{2.4}$$

## 2.5 Energy Conservation

The first law of thermodynamics states that energy can be transformed, but cannot be created or destroyed. Therefore, the energy in the system must be conserved and the rate of energy accumulation must equal the sum of net rate of energy transfer and the rate of internal heat generation inside a unit volume of the medium. This principle applies to both the fluid and the solid, thus energy will be conserved for both the fluid and the solid phase.

Energy transfer in a porous medium is mainly due to conduction and convection. Phase change do not occur in our system, and radiation effects are neglected. Heat conduction is caused by a temperature gradient, hence the conductive heat flux through a medium is $-\kappa\nabla T$ and the net rate of conduction into a unit volume of the medium is $\nabla\cdot(\kappa\nabla T)$. Here, $\kappa$ is the thermal conductivity and $T$ is the temperature of either the fluid or the solid. Convection occured when heat transfer was assisted by the motion of the fluid, so the rate of energy transfer due to convection is $(\rho c_p)_f\mathbf{v}\cdot\nabla T_f$, where $c_p$ is

the specific heat at constant pressure of the fluid. The subscript $f$ refers to the fluid phase. Adding these terms, we obtain the following equations for the conservation of energy in the fluid and the solid phase:

$$\phi(\rho c_p)_f \frac{\partial T_f}{\partial t} + (\rho c_p)_f \mathbf{v} \cdot \nabla T_f = \phi \nabla \cdot (\kappa_f \nabla T_f) + \phi q_f''', \tag{2.5}$$

$$(1-\phi)(\rho c)_s \frac{\partial T_s}{\partial t} = (1-\phi)\nabla \cdot (\kappa_s \nabla T_s) + (1-\phi) q_s''', \tag{2.6}$$

[21]. The subscripts $s$ refers to the solid phase, $c$ is the specific heat of the solid and $q'''$ is heat production per unit volume of the medium.

We now assume local thermal equilibrium; that is, $T_s = T_f = T$, and set the production terms to zero. Setting the production terms to zero is not necessarily the same as assuming no heat production in the system, since heat production may be invoked in the boundary conditions. Adding Equations (2.5) and (2.6) yields

$$(\rho c)_m \frac{\partial T}{\partial t} + (\rho c)_f \mathbf{v} \cdot \nabla T = \nabla \cdot (\kappa_m \nabla T), \tag{2.7}$$

where

$$(\rho c)_m = (1-\phi)(\rho c)_s + \phi(\rho c_p)_f$$
$$\kappa_m = (1-\phi)\kappa_s + \phi \kappa_f.$$

These are, respectively, the overall heat capacity per unit volume and overall thermal conductivity of the fluid and the solid.

# Chapter 3

# Model for Convection Cells

In the former chapter we ended up with three model equations: Darcy's law,

$$\mathbf{v} = -\frac{K}{\mu}(\nabla P + \rho g \mathbf{k}), \tag{3.1}$$

the mass conservation equation,

$$\nabla \cdot \mathbf{v} = 0, \tag{3.2}$$

and the energy conservation equation

$$(\rho c)_m \frac{\partial T}{\partial t} + (\rho c)_f \mathbf{v} \cdot \nabla T = \nabla \cdot (\kappa_m \nabla T). \tag{3.3}$$

These three, along with the equation of state for the fluid density, forms a closed system of equations. Our domain is the porous medium between two vertical, coaxial cylinders with height $h$; the inner cylinder having radius $R_w$ and the outer has radius $R$, see Figure 3.1.

We are using cylindrical coordinates, hence the velocity vector $\mathbf{v}$ is on the form

$$\mathbf{v} = v_r \mathbf{e_r} + v_\theta \mathbf{e}_\theta + v_z \mathbf{k}$$

where $\mathbf{e_r}$ and $\mathbf{e}_\theta$ are unit vectors in the radial and azimuthal direction, respectively. The gradient operator is defined by

$$\nabla T = \frac{\partial T}{\partial r}\mathbf{e_r} + \frac{1}{r}\frac{\partial T}{\partial \theta}\mathbf{e}_\theta + \frac{\partial T}{\partial z}\mathbf{k},$$

and the divergence operator is given by

$$\nabla \cdot \mathbf{v} = \frac{1}{r}\frac{\partial (r v_r)}{\partial r} + \frac{1}{r}\frac{\partial v_\theta}{\partial \theta} + \frac{\partial v_z}{\partial z}.$$

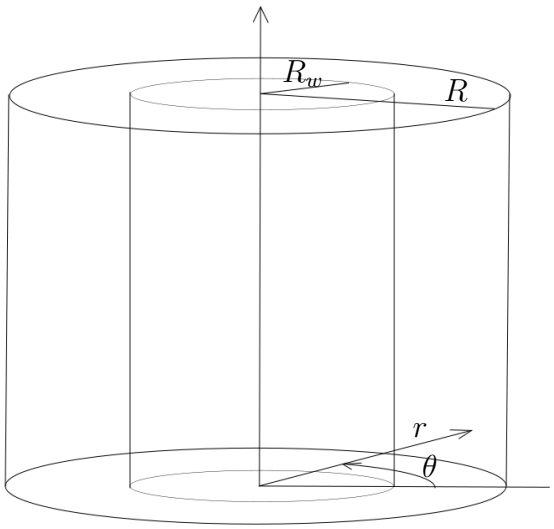


Figure 3.1: Sketch of annular cylinder.

## 3.1 Coordinate Transform

When we solve the system of equations, we are interested in how the solution changes when the parameters are perturbed. Often a perturbation of one parameter affects the system in the same way as another parameter, hence no new information is obtained by changing both parameters. To avoid situations such as this, we nondimensionalize our equations. Making the equations nondimensional helps us note how ratios of parameters affect the solution. In stead of having a large set of parameters, we get a few nondimensional ratios of parameters to vary.

To nondimensionalize the equations, we use a coordinate transform based on the coordinate transform by Lewis and Seetharamau in [19]:

$$r^* = \frac{r}{h};\ z^* = \frac{z}{h};\ v_r^* = \frac{v_r h}{\alpha_f};\ v_\theta^* = \frac{v_\theta h}{\alpha_f};\ v_z^* = \frac{v_z h}{\alpha_f};$$

$$t^* = \frac{t\alpha_f}{\sigma h^2};\ T^* = \frac{T - T_c}{T_w - T_c};\ P^* = \frac{PK}{\mu\alpha_f};$$

Here, $h$ is the height of the cylinder, $\alpha_f = \kappa_m/(\rho c_p)_f$ is thermal diffusivity, and $\sigma = (\rho c)_m/(\rho c_p)_f$ is the ratio of the volumetric heat capacities of medium and fluid. The two temperatures $T_w$ and $T_c$ are reference temperatures and represent a typical temperature difference in the system. Since we are considering a cylinder that is heated from below and cooled from above, $T_w$ and

$T_c$ will be the temperatures of the bottom and the top of the cylinder, respectively. Using the star, $^*$, as a superscript, means that the variable has no dimension.

## 3.2 The Rayleigh Number

Substituting the above nondimensional variables into the equations, will introduce the dimensionless Rayleigh number and Darcy number given by

$$\mathrm{Ra} = \frac{\beta g h^3 (T_w - T_c)}{\nu \alpha_f},$$

and

$$\mathrm{Da} = \frac{K}{h^2},$$

where $\nu = \mu/\rho_f$ is the kinematic viscosity of the fluid. The Rayleigh number indicates whether conduction or natural convection is dominating the system, while the Darcy number characterizes the flow properties of the medium.

The Rayleigh number and Darcy number will in our equations only appear in product with each other, hence we introduce the Rayleigh-Darcy number

$$\mathrm{RaDa} = \mathrm{Ra} * \mathrm{Da} = \frac{\beta g h K (T_w - T_c)}{\nu \alpha_f}. \tag{3.4}$$

For short, we will refer to the Rayleigh-Darcy number as the Rayleigh number and use the notation Ra. Since we never use the actual Rayleigh number, this shouldn't lead to any ambiguity.

We distinguish between the Rayleigh number Ra and the critical Rayleigh number $\mathrm{Ra}_c$. The Rayleigh number depends on flow related properties of the fluid and the porous medium, while the critical Rayleigh number is a constant determined only by the geometry of the domain and the boundary conditions related to the system. When the Rayleigh number is below the critical value, heat transfer is primarily in the form of conduction. When it exceeds the critical value, heat transfer is primarily in the form of convection and convection cells may form.

The critical Rayleigh number can be interpreted as a criterion for onset of convection, and determining the value of the critical Rayleigh number for different geometries and boundary conditions, is important when studying the onset of convection cells.

## 3.3 The Nondimensional Model Equations

Substituting the dimensionsless variables into our model equations yields a new system of equations. Darcy's law (3.1) is transformed into

$$\mathbf{v}^* = -\nabla P^* + \mathrm{Ra} T^* \mathbf{k}, \tag{3.5}$$

the mass conservation equation (3.2) becomes

$$\nabla \cdot \mathbf{v}^* = 0, \tag{3.6}$$

and the energy conservation equation (3.3) becomes

$$\frac{\partial T^*}{\partial t^*} + \mathbf{v}^* \cdot \nabla T^* = \nabla^2 T^*. \tag{3.7}$$

We have inserted the equation of state for the density into the equations when necessery, so we only have five (scalar) equations, and only the five unknowns $\mathbf{v}^*$, $P^*$ and $T^*$. Using nondimensional length scales, the cylinder has height 1, inner radius $R_w^* = R_w/h$ and outer radius $R^* = R/h$.

In the following chapters, only nondimensional variables will be used, so we drop the superscript $^*$ to ease the notation. If dimensional quantities are used, this will be specified in the text.

If we wish to solve the above system of equations, boundary conditions are required. We need boundary conditions on the top and bottom and on both the vertical sidewalls of the cylinder. It is not necessary to use explicit boundary conditions in $\theta$-direction since $2\pi$-periodicity is implicitly assumed for all variables.

We assume the top and bottom of the cylinder to be impermeable and perfectly heat conducting. Impermeable means that no fluid can flow through, or, written mathematically,

$$v_z = 0 \text{ at } z \in \{0, 1\}. \tag{3.8}$$

Perfectly heat conducting means that the top and bottom are held at constant temperatures the whole time. As already mentioned, we assume heating from below and cooling from above, hence,

$$T = 1 \text{ at } z = 0 \tag{3.9}$$

and

$$T = 0 \text{ at } z = 1. \tag{3.10}$$

We further assume the sidewalls of the cylinder to be impermeable:

$$v_r = 0 \text{ at } r \in \{R_w, R\}. \tag{3.11}$$

For the temperature on the sidewalls, we will in the following chapter consider two cases: we either let the sidewalls be perfectly heat conducting, or we choose them to be insulated. When the sidewalls are heat conducting, we assume a linear temperature distribution connecting the temperature difference between the top and bottom of the cylinder. Insulated sidewalls means that there are no heat flow over the vertical boundaries, hence the temperature gradient over the sidewalls has to be zero. These two cases can be written mathematically as

$$T = 1 - z \text{ at } r \in \{R_w, R\} \tag{3.12}$$

when the sidewalls are heat conducting, or

$$\frac{\partial T}{\partial r} = 0 \text{ at } r \in \{R_w, R\} \tag{3.13}$$

when the sidewalls are insulated.

# Chapter 4

# Linear Stability Analysis

The onset of natural convection in saturated porous media is determined by the value of the critical Rayleigh number. The critical Rayleigh number will depend on the geometry of the domain and the boundary conditions of the system.

Various aspects of natural convection in porous media have been investigated in the last half century. The critical Rayleigh number for the onset of natural convection in a uniform horizontal porous layer of infinite extent which is heated from below was determined to be $4\pi^2$ by Horton and Rogers [15] and later Lapwood [18]. Horton, Rogers and Lapwood confined their interest to cases where the upper and lower surfaces are impermeable and perfectly heat conducting, while later work, such as the paper by Nield [20], also investigated permeable upper and lower surfaces subject to constant heat fluxes. A table showing how the critical Rayleigh number and the corresponding wavenumber depends on the type of boundary condition which have been applied may be found in Nield and Bejan [21].

Later works have included enquiries concerning geometries other than horizontally infinite cavities: Beck [4] investigated the case of a finite cuboidal box with insulated and impermeable lateral walls together with perfectly conducting horizontal surfaces. A very similar paper by Wang [31] studies a lower surface subject to a constant heat flux, whilst the upper surface remains perfectly conducting. A circular cylinder with impermeable walls and insulated sidewalls was considered by Zebib [33], and Wang [32] solved the same problem as Zebib but subjected the upper surface to constant temperature and pressure boundary conditions while the lower surface was impermeable but could be held either at a constant temperature or at a constant heat flux. These last two authors presented mode maps in the style of Beck [4]. The case

of a circular cylinder with perfectly conducting boundaries was considered by Haugen and Tyvand [13], who also compared their findings with Zebib's results. In the papers concerning convection in cylinders, the criterion for the onset of convection is given as a function of the radius of the vertical outer boundary. An annular cylindrical cavity with insulated sidewalls was investigated by Bau and Torrance [2]. They allowed the upper surface to be either permeable or impermeable and found criteria for the onset of convection and the preferred mode shapes as functions of the inner and outer radii of the cavity.

To find critical Rayleigh numbers for our annular cylinder with either conducting or insulated sidewalls, we will use linear stability analysis on the three nondimensional model equations (3.5)-(3.7) and apply the boundary conditions (3.8)-(3.13). We will also develop a method for determining the preferred convective modes in order to obtain a mode map.

## 4.1 Linearization Around a Stationary Solution

The equations (3.5)-(3.7) together with the the boundary conditions (3.8)-(3.13) have the steady-state solution

$$T_s = 1 - z,\ \mathbf{v}_s = 0,\ P_s = P_0 + \mathrm{Ra}(z - \frac{z^2}{2}).$$

This stationary solution represents conduction. Owing to the heating from below and cooling from the top we have a linear temperature gradient and there are no fluid flow. For convection to occur, we need a small perturbation of the system, that is,

$$T = T_s + \hat{T},\ \mathbf{v} = \hat{\mathbf{v}},\ P = P_s + \hat{P}, \tag{4.1}$$

where $\hat{T}$, $\hat{\mathbf{v}}$ and $\hat{P}$ are all small quantities. We insert these into the model equations (3.5)-(3.7), obtaining equations for $\hat{T}$, $\hat{\mathbf{v}}$ and $\hat{P}$. Since we are dealing with small quantities, we can neglect all nonlinear terms. Darcy's law for the perturbed velocity is

$$\hat{\mathbf{v}} = -\nabla\hat{P} + \mathrm{Ra}\hat{T}\mathbf{k}. \tag{4.2}$$

The mass conservation equation now reads

$$\nabla \cdot \hat{\mathbf{v}} = 0, \tag{4.3}$$

while the linear version of the energy equation for the perturbed quantities is

$$\frac{\partial \hat{T}}{\partial t} - \hat{v}_z = \nabla^2 \hat{T}. \tag{4.4}$$

We seek an equation in $\hat{T}$ only. To eliminate $\hat{v}_z$ from (4.4), we apply the curl operator on Darcy's law (4.2) twice. The $z$-component of Darcy's law then becomes

$$\nabla^2 \hat{v}_z = \mathrm{Ra} \nabla_1^2 \hat{T}, \tag{4.5}$$

where $\nabla_1^2 = \nabla^2 - \frac{\partial^2}{\partial z^2}$. Since we are only interested in the onset of convection, we can neglect the time dependence in the energy equation (4.4). Combining this with Equation (4.5) yields

$$\nabla^4 \hat{T} + \mathrm{Ra} \nabla_1^2 \hat{T} = 0. \tag{4.6}$$

If we insert the perturbed solution (4.1) into the boundary conditions (3.8)-(3.13), we obtain boundary conditions for the *perturbed* temperatures and velocity. The perturbed vertical velocity must still be zero at the top and bottom of the cylinder;

$$\hat{v}_z = 0 \text{ at } z \in \{0, 1\}, \tag{4.7}$$

while the temperature perturbation must be zero at the top and bottom since the stationary $T_s = 1 - z$ already fulfills the boundary conditions here;

$$\hat{T} = 0 \text{ at } z \in \{0, 1\}. \tag{4.8}$$

For the impermeable vertical sidewalls, the perturbed radial velocity must be zero,

$$\hat{v}_r = 0 \text{ at } r \in \{R_w, R\}. \tag{4.9}$$

When the sidewalls are heat conducting, the temperature perturbation must be zero

$$\hat{T} = 0 \text{ at } r \in \{R_w, R\}. \tag{4.10}$$

For insulated sidewalls, the radial temperature gradient of the temperature perturbation must be zero,

$$\frac{\partial \hat{T}}{\partial r} = 0 \text{ at } r \in \{R_w, R\}. \tag{4.11}$$

Since we obtain an equation in $\hat{T}$ only, that is, Equation (4.6), we need to rewrite the two boundary conditions (4.7) and (4.9). Rewriting (4.7) is easy,

since we can use the linearized energy equation (4.4) with time dependence neglected to obtain

$$\nabla^2 \hat{T} = 0 \text{ at } z \in \{0, 1\}. \tag{4.12}$$

Using the curl of Darcy's law (4.2) and the radial derivative of the linearized energy equation (4.4) with time dependence neglected, we can rewrite (4.9) into

$$\frac{\partial}{\partial r}(\nabla^2 \hat{T} + \mathrm{Ra}\hat{T}) = 0 \text{ at } r \in \{R_w, R\}. \tag{4.13}$$

### 4.1.1 Solution of the Fourth Order Equation

To summarize, we have the fourth order equation (4.6) and the boundary conditions (4.8), (4.12) and (4.13), and one of (4.10) or (4.11). This system is possible to solve using separation of variables. For the details on how to do this, we refer to Appendix A. Applying the boundary conditions in $z$, (4.8) and (4.12), the solution to (4.6) becomes a sum of $\hat{T}_1$ and $\hat{T}_2$, which are given by

$$\hat{T}_1 = \Big[A_m J_m(kr) + B_m Y_m(kr)\Big] \cos(m\theta) \sin(\pi z), \tag{4.14}$$

$$\hat{T}_2 = \Big[C_m J_m\Big(\frac{\pi^2}{k} r\Big) + D_m Y_m\Big(\frac{\pi^2}{k} r\Big)\Big] \cos(m\theta) \sin(\pi z). \tag{4.15}$$

Here, $m$ is a positive integer, $J_m$ and $Y_m$ are Bessel functions of order $m$ and of the first and second kind, respectively, and $k$ is a wavenumber which is related to the Rayleigh number through

$$\mathrm{Ra} = \frac{(k^2 + \pi^2)^2}{k^2}. \tag{4.16}$$

The constants $A_m$, $B_m$, $C_m$ and $D_m$ depend on $m$ and can be found by applying the boundary conditions on the sidewalls, that is, the condition of impermeable sidewalls and the condition of either conducting or insulated sidewalls.

We note that Equation (4.16) is the same relation obtained for the critical Rayleigh number for rolls in an infinitely large porous layer. The smallest value of Ra will be $4\pi^2$ when $k = \pi$.

## 4.2 The Critical Rayleigh Number

If we were to apply the boundary conditions (4.13) and one of (4.10) or (4.11) directly on the perturbed solution $\hat{T}$, we would only get the zero-solution

since the four boundary conditions result in four homogenous, linear equations. To obtain non-zero solutions we demand the determinant of this linear system of equations to be zero. Using this approach we get an eigenvalue problem for the wavenumber $k$. For the conducting sidewalls case, we use the boundary conditions (4.10) and (4.13) and demand

$$\begin{vmatrix} J_m(kR_w) & Y_m(kR_w) & J_m(\frac{\pi^2}{k}R_w) & Y_m(\frac{\pi^2}{k}R_w) \\ \frac{dJ_m}{dr}(kR_w) & \frac{dY_m}{dr}(kR_w) & \frac{dJ_m}{dr}(\frac{\pi^2}{k}R_w) & \frac{dY_m}{dr}(\frac{\pi^2}{k}R_w) \\ J_m(kR) & Y_m(kR) & J_m(\frac{\pi^2}{k}R) & Y_m(\frac{\pi^2}{k}R) \\ \frac{dJ_m}{dr}(kR) & \frac{dY_m}{dr}(kR) & \frac{dJ_m}{dr}(\frac{\pi^2}{k}R) & \frac{dY_m}{dr}(\frac{\pi^2}{k}R) \end{vmatrix} = 0. \tag{4.17}$$

For each value of $R_w$ and $R$, and for each $m$, there will be an infinite number of solutions $k$, denoted $k_{m,n}$. We seek the value of $k_{m,n}$ that minimizes the Rayleigh number, hence also providing the critical Rayleigh number using Equation (4.16):

$$\mathrm{Ra}_c = \min_{m,n}\Big[\frac{(k_{m,n}^2 + \pi^2)^2}{k_{m,n}^2}\Big]. \tag{4.18}$$

The $n$-enumeration is a manner of separating the different solutions of Equation (4.17) and has no apparent physical meaning. Since the minimum of the Rayleigh number will occur for the $k_{m,n}$ closest to $\pi$, we can arrange the $k_{m,n}$'s such that the one closest to $\pi$ is number 1, the second closest number 2 and so on. When minimizing Equation (4.18), we always end up choosing one of the $k_{m,1}$, and consequently we need only search over the $m$'s when searching for the critial Rayleigh number.

For the insulated sidewalls we apply the boundary conditions (4.11) and (4.13) and the resulting eigenvalue problem for $k$ may be simplified into

$$\frac{dJ_m}{dr}(kR_w)\frac{dY_m}{dr}(kR) - \frac{dJ_m}{dr}(kR)\frac{dY_m}{dr}(kR_w) = 0. \tag{4.19}$$

As for the conducting case, we search for the $k_{m,1}$ that minimizes the Rayleigh number.

For both the conducting and insulated sidewalls case, and for each value of $R_w$ and $R$, we are able to find the critical Rayleigh number by minimizing Equation (4.18) over the eigenvalues $k_{m,1}$. Hence we can plot the critical Rayleigh number as a function of $R_w$ and $R$.

## 4.3 Convection Modes

Different convective patterns may occur when convection is present in a porous medium. For our two coaxial cylinders, there may be flow vortices stretching around the inner radius in azimuthal direction, vortices orthogonal to the vertical sidewalls in radial direction, or combinations of these. The specific convection patterns are called convective modes. Given a domain along with boundary conditions and with a Rayleigh number slightly above the critical, a certain convective mode will appear. Using the results from the linear stability analysis, it is possible to predict which convective mode will occur. We will now outline a strategy on how to find these convective modes and we explain in more detail how these convective modes behave.

### 4.3.1 Vortices in Azimuthal or Radial Direction

When we searched for the critical Rayleigh number, a wavenumber $k_{m,1}$ was found. This wavenumber can help us determine the preferred convective mode at the onset of convection, since the value of $m$ in the $k_{m,1}$ that minimizes the Rayleigh number, is the same $m$ occuring in the Equations (4.14) and (4.15) for the perturbed temperature. The value of $m$ decides the number of vortices in the azimuthal direction because of the $\cos(m\theta)$ term. For example, if $m = 1$ turns out to give the critical Rayleigh number, the temperature distribution in the azimuthal direction will be shaped like a $\cos(\theta)$. When investigating the streamlines, this temperature profile corresponds to two adjacent vortices, see Figure 4.1. In general there will be $2m$ vortices in the azimuthal direction.

To find the number of vortices in the radial direction, we can calculate the radial component of $v_z$ using the linearized energy equation (4.4) with time dependence neglected. With $\hat{T}$ being known, finding the radial component of $\hat{v}_z$ is only a matter of differentiating $\hat{T}$ and neglecting contributions from $z$ and $\theta$. Since the steady state solution of the velocity vector is zero, the total velocity profile will equal the perturbed velocity field, that is, $v_z = \hat{v}_z$. By investigating the number of sign changes in $v_z$ between $r = R_w$ and $r = R$, the number of radial vortices can be found; every zero of $v_z$ corresponds to the top and bottom of a convection cell, see Figure 4.2. Therefore, if there are $p$ sign changes in the radial component of $v_z$, then $p$ vortices in radial direction is present[1].

[1]The author would like to acknowledge Professor D. Andrew S. Rees for suggesting this approach of determining $p$.

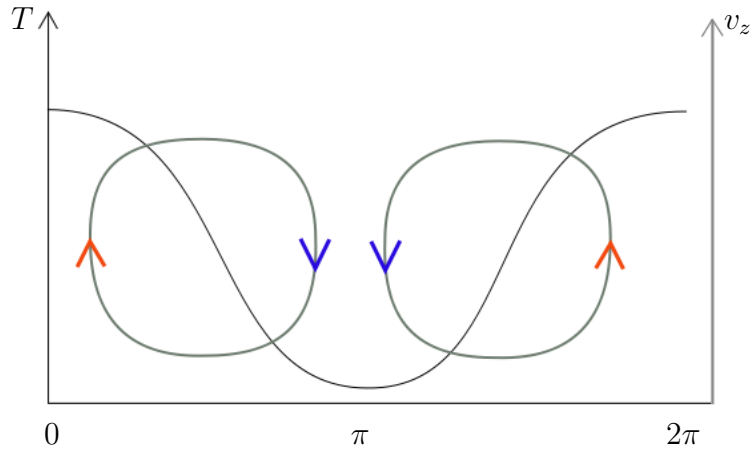


Figure 4.1: Increasing temperature means the warm lower fluid is flowing upwards. Lower temperature means the cool upper fluid is flowing downwards.

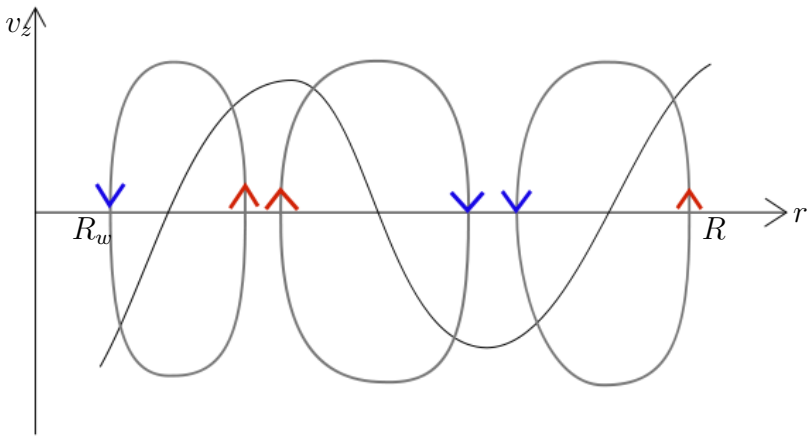


Figure 4.2: Negative $v_z$ corresponds to declining stream lines while positive $v_z$ corresponds to upward stream lines. A sign change in the vertical velocity profile marks the top and bottom of a convection cell.

Since we only have convection cells in radial and azimuthal direction, we can associate a convective pattern with the numbers $(m, p)$. For each value of the inner radius $R_w$ and the outer radius $R$, there will be a unique stable mode $(m, p)$ when the Rayleigh number is slightly above the critical. We can make a *mode map* over which convective mode corresponds to each $R_w$ and $R$ using the method sketched above.

When the Rayleigh number is just slightly larger than the critical Rayleigh number, the system will prefer the mode $(m, p)$. But, it is possible to include several critical Rayleigh numbers and hence several possibly stable modes. The idea is as following: when we minimized over the $k_m$ to find $\mathrm{Ra}_c$, we found the *smallest* Rayleigh number and the corresponding mode $(m, p)$. But if we also found the *second smallest* Rayleigh number, denoted $\mathrm{Ra}_{c,2}$, and corresponding mode $(m_2, p_2)$, then this mode too should be possible when the Rayleigh number is larger than $\mathrm{Ra}_{c,2}$. We may continue the process finding $\mathrm{Ra}_{c,3}$ with corresponding $(m_3, p_3)$ and so on. In theory, when the Rayleigh number is larger than $\mathrm{Ra}_{c,n}$ for some positive integer $n$, then all modes $(m, p)$, $(m_2, p_2)$, $(m_3, p_3)$, ..., $(m_n, p_n)$ are possible. In practice, we don't know whether the different modes are stable and which will be preferred, but this can be established through simulations.

### 4.3.2 The Convective Structure and Mode Maps

To better understand how a mode $(m, p)$ will look like, some simple plots of the flow patterns can be used to illustrate. The mode $(1, 0)$, which has two adjacent convection cells in azimuthal direction and no convection cells in radial direction, will behave as illustrated in Figure 4.3. The mode $(0, 1)$ is axisymmetric since $m = 0$, and will look like as in Figure 4.4. If more convection cells are present in the radial direction, these will be adjacent as illustrated in Figure 4.2 above. More complex modes will be combinations of these two basic convection patterns, as in Figure 4.5 which illustrates the convective mode $(1, 1)$ and Figure 4.6 illustrating $(2, 1)$. In the following figures, the colours describe the vertical velocity; lighter colours indicate larger, positive velocities, while dark colours indicate larger (in magnitude), negative velocities. The arrows are the horizontal velocities seen from above.

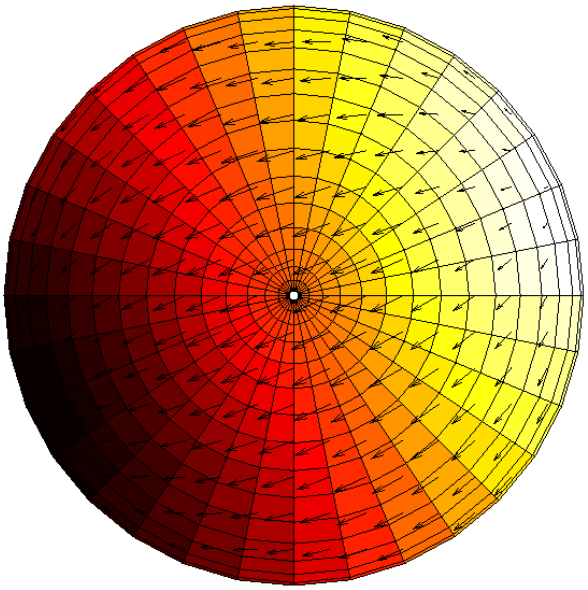

Figure 4.3: The mode $(1, 0)$.

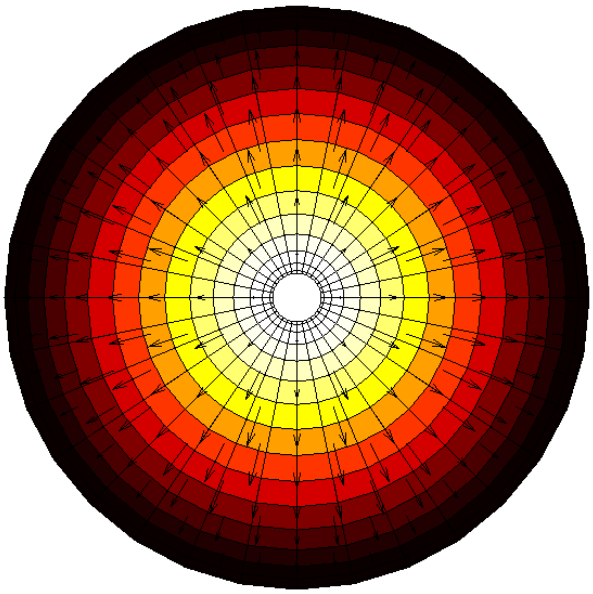

Figure 4.4: The mode $(0, 1)$.

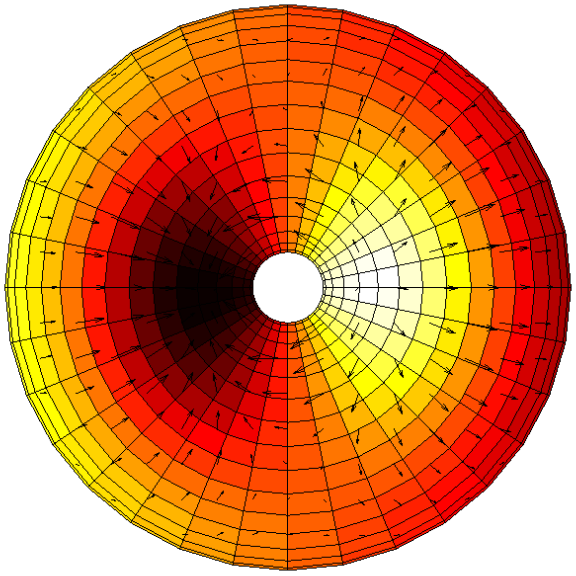

Figure 4.5: The mode $(1, 1)$.

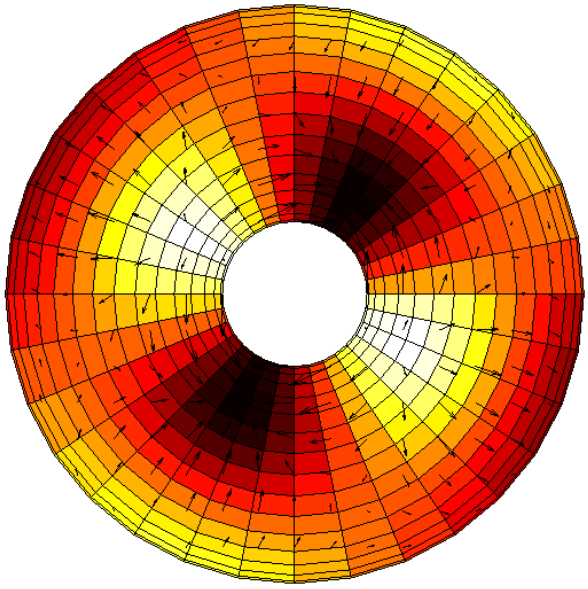

Figure 4.6: The mode $(2, 1)$.

# Chapter 5

# Results and Discussion - Linear Stability Analysis

Using the theory and methods described in Chapter 4, we search for the critical Rayleigh numbers and corresponding mode maps for the cases of sidewalls being heat conducting and insulated. We also find the higher order Rayleigh numbers and corresponding modes, and investigate the case of the inner radius approaching zero. In the following, we have restricted ourselves to only consider values of the inner radius between 0 and 2, and values of the outer radius between 0 and 4.

## 5.1 Critical Rayleigh Number

We have found the critical Rayleigh numbers for both the conducting and insulated sidewalls. The results are presented using contour plots. We also try to explaine the results and compare them with previous results by Haugen and Tyvand [13] (conducting cylinder without annulus), Zebib [33] (insulated cylinder without annulus) and Bau and Torrance [2] (insulated annular cylinder).

### 5.1.1 Conducting Sidewalls

For the conducting sidewalls, the critical Rayleigh number decreases monotonically as the outer radius $R$ increases, while it increases as the inner radius $R_w$ increases with $R$ held fixed, see Figure 5.1 for contour plot. For fixed values of $R_w$, the critical Rayleigh number reduces towards $4\pi^2$ as $R$ increases. The small bumps in the contour plot corresponds to transitions from one convective mode to another.

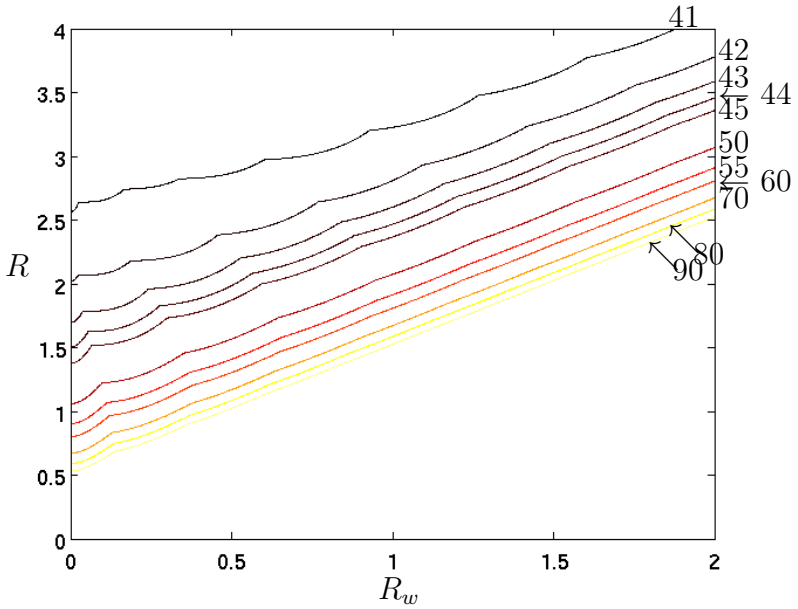


Figure 5.1: Critical Rayleigh number for conducting sidewalls.

Haugen and Tyvand [13], who considered a circular cylinder of porous medium with a perfectly heat conducting sidewall, showed that the critical Rayleigh number is a monotonically decreasing function of $R$ and it decreases towards $4\pi^2$ when $R \to \infty$. For fixed nonzero values of $R_w$ our results are in qualitative agreement. Both [13] and [25] showed that a conducting sidewall does not correspond to a natural cell boundary, and that cells near such a boundary are wider than their insulating sidewall counterparts. Thus a larger value of $R$ means that an increasing amount of the porous cavity is unaffected by the presence of the boundary. The presence of the inner cylinder does not change this fact and provides a further restriction to convective flow. When the outer radius, $R$, is held fixed and the inner radius, $R_w$, is increased, the critical Rayleigh number increases since the two conducting sidewalls are now closer together, restraining the convection even more. Therefore it is no surprise that the critical Rayleigh numbers found here for chosen values of the outer radius are always larger than those given by Haugen and Tyvand.

Letting $R_w$ approach zero provides the same values of the critical Rayleigh number as the ones found by Haugen and Tyvand. See Section 5.4 for more details on this subject.

### 5.1.2 Insulated Sidewalls

For the insulated sidewalls, the function describing the critical Rayleigh number has several local maxima and minima, see Figure 5.2. The maxima occur when the system goes from one preferred convection mode to another, while the minima, all giving a critical Rayleigh number of $4\pi^2$, occur in between the mode transitions. For increasing values of $R$, with $R_w$ fixed, the critical Rayleigh number will converge towards $4\pi^2$ in the sense that all the local maxima decay towards $4\pi^2$. The convergence rate is faster than for the conducting sidewalls.

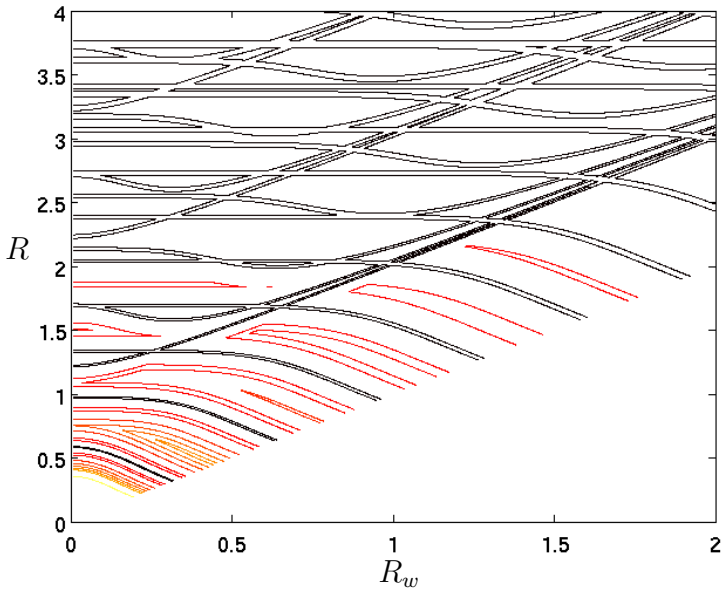


Figure 5.2: Contour plot of the critical Rayleigh number as a function of $R_w$ and $R$ when the sidewalls are insulated. The black lines are contours slightly over $4\pi^2$, the red lines indicate Rayleigh value 40, while the lighter colours represent values in the range from 41 to 55.

As we will observe in the next section, all local maxima of the critical Rayleigh number surface occur when a shift from one preferred mode to another is made, while the local minima happens in the middle of a mode's part of the domain. The physical explanation behind this phenomenon, is the idea of fitting convection cells inside a given porous annular cylinder. The "boundary" between two convection cells is virtually a heat insulated and impermeable internal boundary since there will be no heat or fluid flow between two separate

convection cells. Hence, the inner and outer sidewalls can be interpreted as the boundary of other convection cells. The convection cells distribute inside the porous medium made available for them - the vertical internal boundaries between different convection cells do not remove buoyancy as in the heat conducting sidewalls case. A convection cell can be interpreted as a geometric object having (in our case) height 1, and some horizontal extent and will have an ideal horizontal extent in an infinite porous layer. Certain values of inner and outer radii will correspond to some number of convection cells of ideal size managing to distribute inside the porous medium and these values of inner and outer radii will give a critical Rayleigh number of $4\pi^2$. Changing the inner and outer radius just slightly - either increasing or decreasing - causes the convection cells to rescale themselves, hence the ideal size is no longer obtained and the critical Rayleigh number increases. The critical Rayleigh number will continue to increase until another distribution of convection cells is more appropriate, whereupon the critical Rayleigh number will decrease. When the outer radius increases, the available porous media is so large that many convection modes can obtain an ideal cell distribution. Hence the critical Rayleigh number converges towards $4\pi^2$.

Both Zebib [33] (cylinder) and Bau and Torrance [2] (annular cylinder) found the critical Rayleigh number to have several maxima and minima when the sidewalls are insulated. The critical Rayleigh numbers found here are in general the same as in the paper of Bau and Torrance, but substantially more values of $R_w$ and $R$ are being considered in this thesis. Using a very small inner cylinder, we obtain the same critical Rayleigh numbers as found by Zebib, and we return to this subject in Section 5.4.

### 5.1.3 Comparison Between the Conducting and the Insulated Sidewalls

For any choice of values $R_w$ and $R$, the critical Rayleigh number will be larger for the conducting sidewalls than for the insulated sidewalls. Haugen and Tyvand [13] observed the same for their non-annular cylinder and explained this by heat conduction being stabilizing as it takes away buoyancy. The presence of an inner cylinder does not change this fact, but in stead we see that a large value of the inner radius increase the critical Rayleigh number even further in the conducting sidewalls case, as more buoyancy is taken away. In the insulated sidewalls case, the effect of an inner cylinder on the critical Rayleigh number is not that large. As for the non-annular sylinder in Zebib's case, we observe several maxima and minima related to jumps

between different convection mode, but we do not observe a large increase on the critical Rayleigh number when $R$ is fixed and $R_w$ increases.

## 5.2 Mode Maps

### 5.2.1 Conducting Sidewalls

The preferred convective mode have been found for both the conducting and insulated sidewalls. For the conducting sidewalls, the value of $m$ increases when the inner radius $R_w$ increases and the outer radius $R$ is held fixed; see Figure 5.3. Although not visible in the Figure, $m$ will become zero when $R_w$ approaches zero. The value of $p$ is zero when the outer radius is not much larger than the inner radius, while for larger values of $R$, we get larger values of $p$.

An increasing value of $m$ for increasing inner radius when the outer radius is held fixed, means that we get more convection cells in the azimuthal direction for a larger inner radius. This is reasonable since, for $R$ held fixed, an increasing $R_w$ means that the porous media is getting more narrow and it is more convenient for the water to flow in the azimuthal direction than in the radial since the closeness of the inner and outer sidewalls takes away buoyancy. Also, it is hard for the convection cells to stretch around the inner cylinder, hence we get many small convection cells in stead of a few large. The increase of $p$ can be explained in a similar manner. When the outer radius is only slightly larger than the inner radius, the narrowness of the porous media makes it difficult for convection cells in the radial direction to appear. A wider porous media encourages convection cells in the radial direction to appear and $p$ increases.

### 5.2.2 Insulated Sidewalls

For insulated sidewalls, we find a complex pattern that delineates the regions where different modes are preferred; see Figure 5.4. The pattern is impossible to describe except in general terms. It is clear that the overall pattern in terms of $m$ has a banded structure where narrow bands exist at certain discrete values of $R - R_w$, which is the width of the annular cavity. When this width is sufficiently small the number of cells in the azimuthal direction increases as $R_w$ increases, and they also correspond to $p = 0$ implying that the cells have little radial dependence.

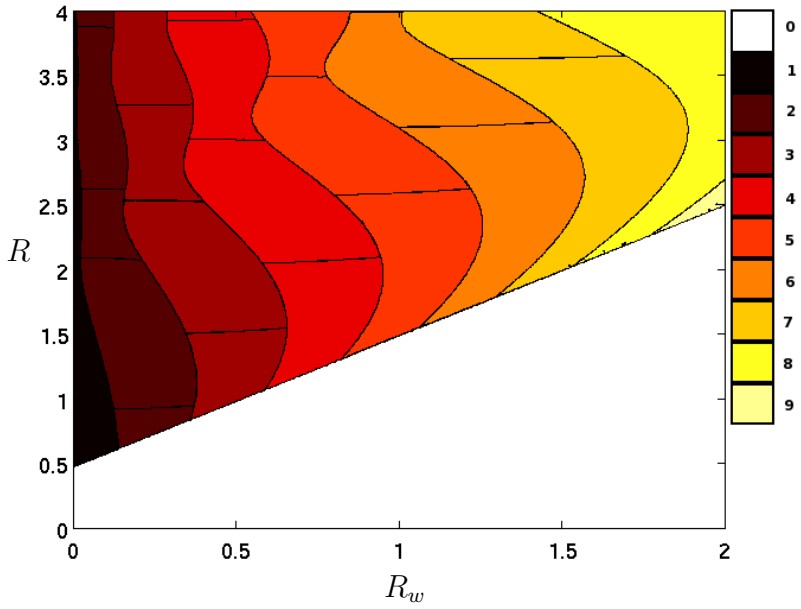


(a) The values of $m$.

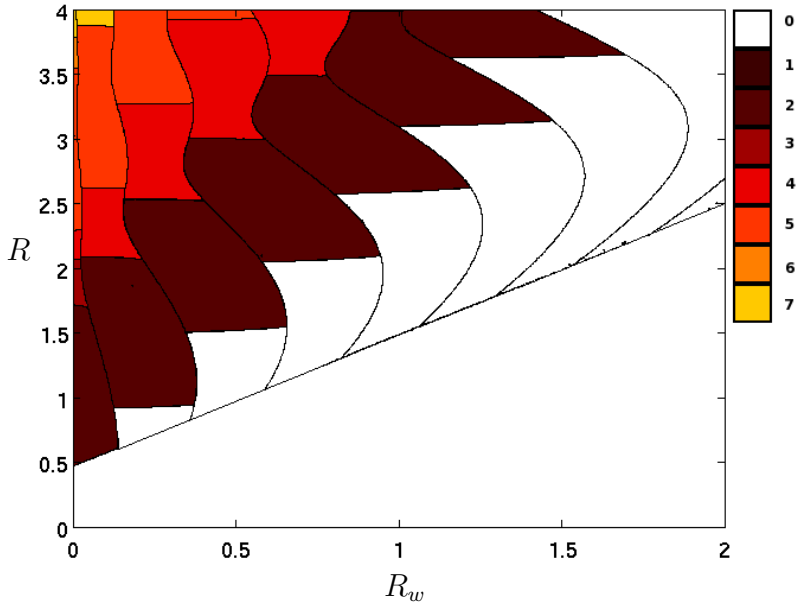


(b) The values of $p$.

Figure 5.3: Mode map for the conducting sidewalls case. The bifurcation trajectories are highlighted with black lines.

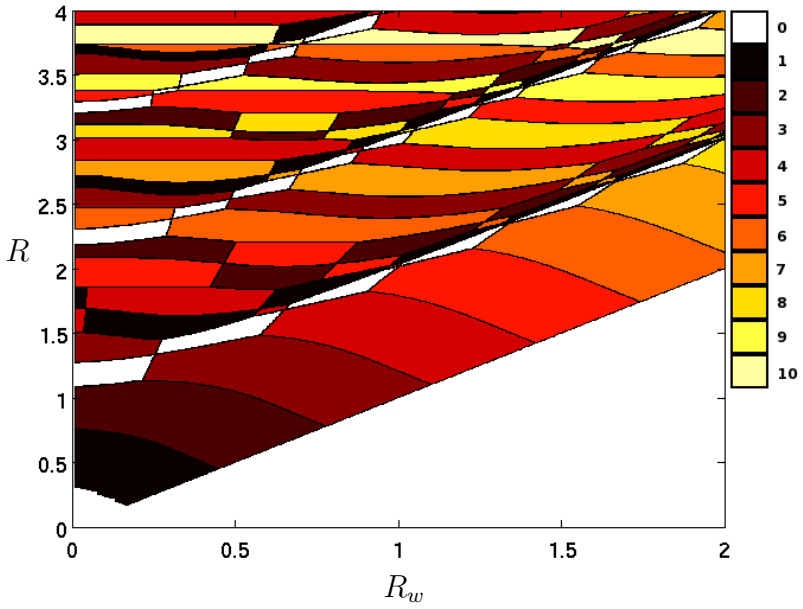


(a) The values of $m$

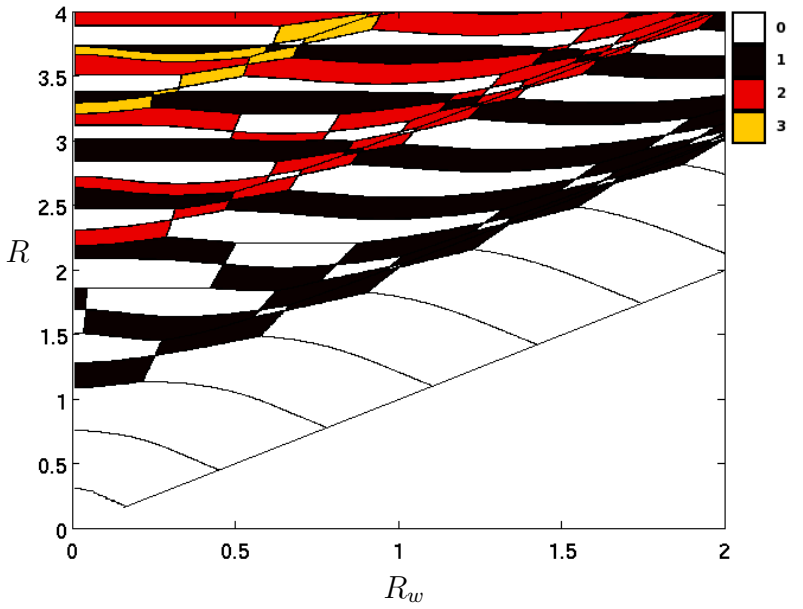


(b) The values of $p$

Figure 5.4: Mode map for the insulated sidewalls case.

These values of $m$ and $p$ have also been found by Bau and Torrance [2], and they made a similar mode map with the inner radius on the x-axis and the quotient between the outer and the inner radius on the y-axis. Converting our plot in the same manner enables us to compare our mode map with the one made by Bau and Torrance, see Figure 5.5. Note that the notation of Bau and Torrance is slightly different from ours; their mode $(m, p)$ correspond to $(m, p-1)$ in our notation.

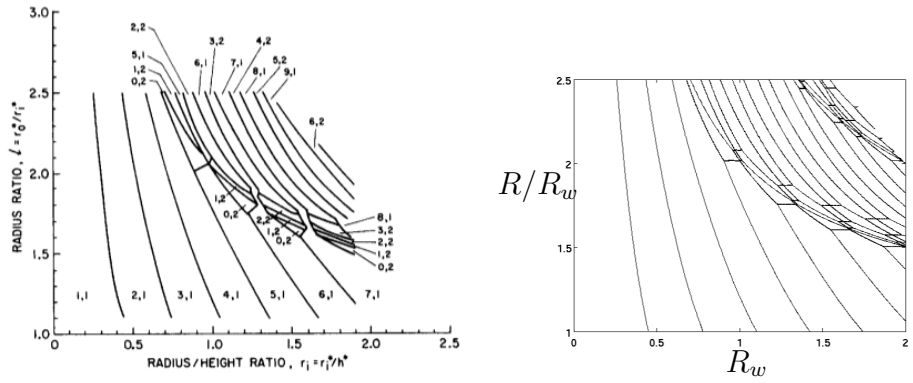


(a) Mode map made by Bau and Torrance. This figure is a copy of Figure 3 in [2].

(b) Our version of the Bau and Torrance mode map

Figure 5.5: Corresponding mode maps for the insulated sidewalls case.

We have in general found the same modes as Bau and Torrance, hence we have not named our modes in the figure. We find more details in the mode map than obtained by Bau and Torrance, and simulations confirm these results. Bau and Torrance do not explain in detail how they obtained their mode map, but we can conclude that their method was not adequate. Bau and Torrance concluded that the preferred convection modes are predominantly asymmetric, that is, $m$ is nonzero. In this study, we also find $m$ to be nonzero in general, but several axisymmetric convection modes are found. Hence, we cannot support Bau and Torrance's conclusion of preferred modes being predominantly asymmetric.

## 5.3 Higher Order Modes

This far we have concentrated only on primary modes, i.e. those which minimize the Rayleigh number, but higher modes also exist and these have to

be computed as part of the minimization procedure for Ra. For any positive integer $n$, we denote the $n^{th}$ order Rayleigh numbers by $\mathrm{Ra}_{c,n}$, where $\mathrm{Ra}_{c,1}$ is the overall critical Rayleigh number. We note that, for both conducting and insulated sidewalls, these higher order Rayleigh numbers which are larger than the critical Rayleigh number, also vary with $R$ and $R_w$, but they converge towards $4\pi^2$ at the same rate as in the same speed as for the primary mode.

$\mathrm{Ra}_{c,n}$ will be equal to $\mathrm{Ra}_{c,n+1}$ at the bifurcation trajectories in the mode map for $(m_n, p_n)$. For increasing $R$, this occur more frequently, meaning that higher order modes are clustered. See Figure 5.6 for the difference between the second and first order critical Rayleigh numbers.

## 5.4 The Limiting Case when $R_w$ Goes to Zero

Zebib [33] and Haugen and Tyvand [13] undertook linear stability analyses similar to ours for a circular (rather than an annular) cylinder. Their cylinders had insulated and heat conducting sidewalls, respectively. In our eigenvalue problems the dispersion relations given by Equations (4.17) and (4.19) may be studied in the limit as the inner radius approaches zero in order to determine if our case reduces to those of Zebib and of Haugen and Tyvand.

Letting the inner radius approach zero in (4.17) and (4.19) is not straightforward since the Bessel functions of second kind, $Y_m$, are singular at zero. The function $Y_m(x)$ behaves as $O(x^{-m})$ as $x \to 0$, except for $Y_0(x)$ which behaves as $O(\ln(x))$. The derivatives $Y'_m(x)$ behave as $O(x^{-m-1})$. On the other hand Bessel functions of the first kind are nonsingular and have nonsingular derivatives at zero.

The determinant in (4.17) includes a term which involves the factor $[Y'_m(kR_w)Y_m(\frac{\pi^2}{k}R_w) - Y_m(kR_w)Y'_m(\frac{\pi^2}{k}R_w)]$. This term will dominate all the others when $R_w$ approaches zero. Hence this term must be set to zero, thereby yielding the condition,

$$J_m(kR)J'_m\Big(\frac{\pi^2}{k}R\Big) - J'_m(kR)J_m\Big(\frac{\pi^2}{k}R\Big) = 0, \tag{5.1}$$

which is the same as that obtained by Haugen and Tyvand in their analysis. Haugen and Tyvand found $m = 0$ to be the preferred convective mode for all $R$. Applying a Taylor series expansion of the determinant (4.17) with $m = 0$ yields terms of $O(\ln(R_w)/R_w)$, $O(1/R_w)$, $O(R_w)$ and higher order terms. The $O(\ln(R_w)/R_w)$-term is the one corresponding to Equation (5.1).

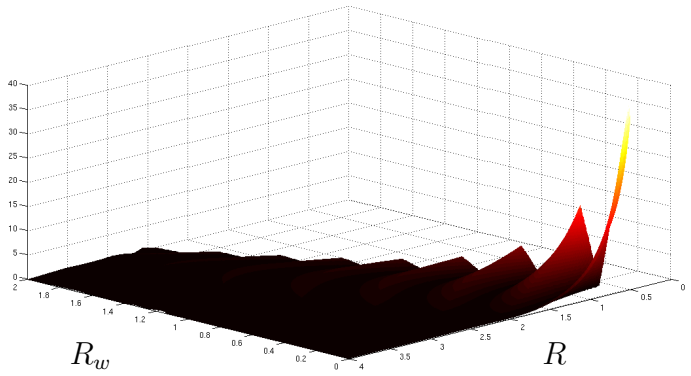


(a) Conducting sidewalls.

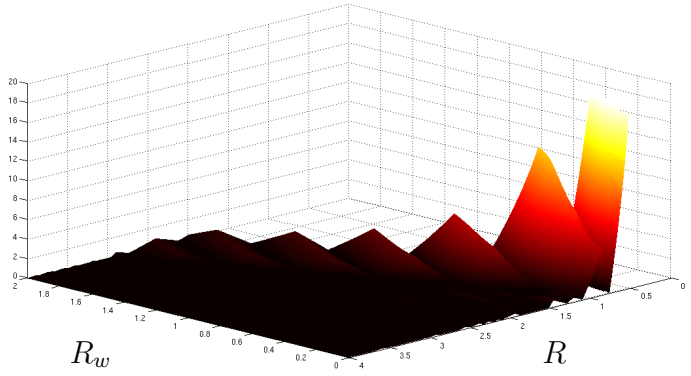


(b) Insulated sidewalls.

Figure 5.6: Difference between $\mathrm{Ra}_c$ and $\mathrm{Ra}_{c,2}$.

We now let $k^0$ be the wavenumbers obtained by Haugen and Tyvand, and $k$ be the wavenumber obtained by us using a small value of $R_w$ and apply a first order Taylor series around $k^0$ in Equation (4.17) in order to balance the $O(1/R_w)$-term. Using this approach, we conclude $k = k^0 + O(1/\ln(R_w))$ as $R_w$ approaches zero and this choice of $k$ implies that

$$\mathrm{Ra}_c = \mathrm{Ra}_c^0 + O(1/\ln(R_w)), \tag{5.2}$$

where $\mathrm{Ra}_c^0$ are the critical Rayleigh numbers found by Haugen and Tyvand. Hence, our critical Rayleigh numbers will approach the Rayleigh numbers found by Haugen and Tyvand as $O(1/\ln(R_w))$ when $R_w$ goes to zero and we may consider the cylinder studied by Haugen and Tyvand as a special case

of the annular cylinder case when the inner radius approaches zero.

Letting $R_w$ approach zero in (4.19) will cause the second term, $J'_m(kR)Y'_m(kR_w)$, to dominate the equation, hence we need

$$J'_m(kR) = 0, \tag{5.3}$$

which is the same equation obtained by Zebib. We apply a first order Taylor series expansion to Equation (4.19) around $k = k^0 + O(R_w^{2m})$ when $m \neq 0$ and around $k = k^0 + O(R_w^2)$ when $m = 0$ as $R_w$ approaches zero. Here $k^0$ are the corresponding wavenumbers found by Zebib and $k$ are the wavenumbers found by us using a small value of $R_w$. This approach will balance all terms in Equation (4.19), hence implying that

$$\mathrm{Ra}_c = \mathrm{Ra}_c^0 + O(R_w^{2m}) \tag{5.4}$$

when $m \neq 0$ and

$$\mathrm{Ra}_c = \mathrm{Ra}_c^0 + O(R_w^2) \tag{5.5}$$

when $m = 0$[1]. Here $\mathrm{Ra}_c^0$ are the critical Rayleigh numbers found by Zebib for a non-annular cylinder. Using $R_w = 10^{-4}$, our critical Rayleigh numbers was approximately the same as the ones found by Zebib, see Figure 5.7, and we found the same preferred convective modes. Hence, a very small inner radius does not affect the results in a significant manner and we regard the problem studied by Zebib as a special case of our analysis.

Figure 5.7 shows the difference between the critical Rayleigh number for circular cylindrical configuration of [13] and the present annular cylinder with $R_w = 10^{-4}$. Despite the inner radius being very small, there remains a strong effect in terms of the critical Rayleigh number. However, the above analysis shows that this difference tends to zero as the inner radius shrinks further.

[1]The author would like to acknowledge Professor D. Andrew S. Rees for performing the analysis resulting in the three relations (5.2), (5.4) and (5.5).

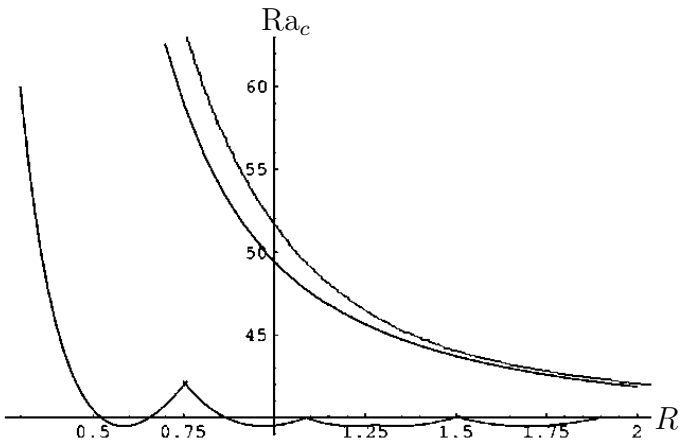


Figure 5.7: Variation of $\mathrm{Ra}_c$ with $R$ for (i) circular cylinder with an insulated sidewall ([33], lowest curve), (ii) circular cylinder with a perfectly conducting sidewall ([13], middle curve), (iii) annular cylinder with perfectly conducting sidewalls and with $R_w = 10^{-4}$. (The figure is adapted from Figure 1 in [13]).

# Chapter 6

# Numerical Model - Spectral Methods

Up to now we have only considered the linear regime of the convection cells. Investigating the time-dependent nonlinear equations would provide information concerning how the nonlinear regime differs from that of the linearized system. The linear theory provides information about the onset mode, but solving the original partial differential equations (3.5)-(3.7) allows us to determine how far into the nonlinear regime this onset mode persists as the favoured mode. Solving the original equations can also provide information about the stability of existing convection cells.

When solving partial differential equations, it is rarely possible to obtain an analytical solution. In stead, a numerical method must be used to find an approximate solution. The main idea behind numerical methods is to discretize the equations and use a computer to solve the discrete version of the system. Several numerical methods exist, and which to choose depends on the properties of the equations you wish to solve, and the sought properties for the approximate solution. The most common numerical methods are the finite difference methods (FDM), the finite element method (FEM) and spectral methods. The FDM replace derivatives in a differential equation with differences, hence leading to a difference equation which is easily solved for one-dimensional domains. However, the accuracy is in general not good. The finite element method's approach is to rewrite the differential equation using variational formulation and then search for a solution in a finite dimensional space which normally consists of piecewise linear functions having local support. The FEM is suitable for complex and multidimensional domains, but the convergence is not always sufficient.

Spectral methods is a class of methods whose main purpose is to approximate the solution using linear combinations of continuous functions existing on the whole domain. When applicable, spectral methods have excellent error properties in the form of an exponential convergence rate. In order to describe the convection cells in three spatial dimensions, good accuracy and fast convergence is essential, hence spectral methods are preferred. The following presentation of spectral methods is based on the books of Trefethen [29] and Boyd [6].

## 6.1 Introduction to Spectral Methods

Spectral methods can be divided into two groups: Galerkin spectral methods and pseudospectral/collocation methods. Similar for both methods is the assumption that the unknown solution $u(x)$ may be approximated by a sum of $(N+1)$ basis functions $\phi_i(x)$ which span the space where the approximate solution exists:

$$u(x) \approx u_N(x) = \sum_{i=0}^{N} a_i \phi_i(x). \tag{6.1}$$

This series is then substituted into the differential equation

$$Lu = f(x),$$

where $L$ is the differential operator. The goal of the spectral methods is to choose the coefficients $\{a_i\}$ such that the residual defined by

$$R(x; a_0, a_1, \ldots, a_N) = Lu_N - f \tag{6.2}$$

is minimized. The essential difference between Galerkin spectral and pseudospectral methods lie in their minimization strategies.

### 6.1.1 Outline of Galerkin Spectral Methods

For the Galerkin spectral method, basis functions that are ortonormal with respect to some inner product is chosen. Any function $g(x)$ lying in the space spanned by $(N+1)$ basis functions may then be expanded as a series,

$$g(x) = \sum_{i=0}^{N} c_i \phi_i(x),$$

where the coefficients $\{c_i\}$ are given by

$$c_i = (\phi_i, g) = \int_a^b \phi_i(x) g(x) \omega(x) dx. \tag{6.3}$$

This is the inner product of $\phi_i(x)$ and $g(x)$ with respect to the weight function $\omega(x)$ on the interval $[a, b]$. The residual function (6.2) may also be expanded as a series of the basis function; hence,

$$R(x; a_0, a_1, \ldots, a_N) = \sum_{i=0}^{\infty} r_i(a_0, a_1, \ldots, a_N)\phi_i(x) \tag{6.4}$$

where the coefficients $\{r_i\}$ are given by the inner product (6.3). The Galerkin method demands the first $(N+1)$ terms of the series (6.4) to be zero. Having a good choice of basis functions, the remaining terms in the series will be small, and an optimum choice of basis functions will lead to the residual converging to zero exponentially fast as $N$ goes to infinity [12]. For a linear differential operator $L$, demanding the $\{r_i\}_{i=0}^{N}$ to be zero, written in matrix notation, corresponds to

$$\mathbf{Ax} = \mathbf{b},$$

where $\mathbf{A}$ is the $(N+1) \times (N+1)$ matrix with entries given by

$$A_{ij} = (\phi_i, L\phi_j),$$

the $(N+1)$ vector $\mathbf{b}$ has the entries

$$b_i = (\phi_i, f) \tag{6.5}$$

and the vector $\mathbf{x}$ consists of the unknown coefficients $\{a_i\}$ which approximate the solution using (6.1). If the problem also has boundary conditions, these are applied by removing the last lines in the matrix, hence loosing some of the accuracy, and substitute the boundary conditions explicitly. For example, the Dirichlet boundary condition $u(x_D) = u_D$ at the boundary point $x = x_D$, leads to the substitution

$$u(x_D) \approx u_N(x_D) = \sum_{i=0}^{N} a_i\phi_i(x_D) = u_D.$$

Neumann boundary conditions are handled by differentiating the basis functions.

### 6.1.2 Outline of Pseudospectral Methods

For the pseudospectral/collocation methods, we demand the residual to be zero in $(N+1)$ collocation points $\{x_i\}$; that is,

$$R(x_i; a_0, a_1, \ldots, a_N) = 0, \quad i = 0, \ldots, N.$$

Recalling how the residual was defined, this leads to the linear system of equations

$$\mathbf{Ax} = \mathbf{b},$$

when $L$ is linear. Here, $\mathbf{A}$ is the $(N+1) \times (N+1)$ matrix with entries given by

$$A_{ij} = LC_j(x_i),$$

where the cardinal functions $C_j$[1] are interpolating functions having value 1 in one collocation point, and 0 in the others, that is;

$$C_j(x_i) = \delta_{ij}. \tag{6.6}$$

The $(N+1)$ vector $\mathbf{b}$ has entries

$$b_i = f(x_i).$$

Basing the matrix equation on the cardinal functions in stead of the usual basis functions means that the unknown vector $\mathbf{x}$ consists of the function values of the approximated solution $u_N$ in the nodes $\{x_i\}$. Each line in the matrix equation represents an equation for the function value in a specific node. Boundary conditions are handled by finding the nodes corresponding to where the different boundary conditions are applied, and substitute the matrix lines with the boundary condtions in these points. More details on how to deal with boundary conditions and how you should choose the collocation points will be explained later.

### 6.1.3 Pros and Cons for Galerkin Spectral and Pseudospectral Methods

Both the Galerkin spectral and pseudospectral methods have their pros and cons. They both have the advantage that low values of N give high accuracy in the resulting approximation compared to the finite elements and the finite difference, but there are differences between the two methods.

The Galerkin spectral methods has its strong point in the use of ortonormal basis functions as there usually will be reccurence formulas for the derivatives of the basis functions, which then leads to the resulting matrix $\mathbf{A}$ being

[1]Note that in the literature, there are "two" types of pseudospectral methods: One where the resulting matrix system solves for the unknown series coefficients $\{a_i\}$ as in the Galerkin spectral method, and the method sketched here which uses Cardinal functions in stead of the normal basis functions and solves for the unknown function values in the collocations points.

banded. Banded matrices are a lot cheaper to solve, which is important when large values of $N$ is used. On the other hand, the need of evaluating the integrals $(f, \phi_i)$ on the right-hand side (6.5) slows the method. Normally one relies on numerical integration to approximate these integrals, but numerical integration procedures are expensive; especially since you need very good estimates on the integrals to maintain high accuracy in the method.

For pseudospectral methods, no numerical integration is needed. The right hand side is just function evalutions of $f(x)$, which in general will be cheap to evaluate. Because of the structure of the linear system, pseudospectral methods are known for being easier to implement. Boundary conditions will also be easier to implement, which is important when more advanced types of boundary conditions are applied. The main disadvantage with pseudospectral is that the resulting matrix will be full. Full matrices are costly to invert, but this is not regarded as a large problem since one normally solves relatively small matrices. Another disadvantage with the pseudospectral methods is the accuracy being slightly smaller compared to the Galerkin spectral methods. The Galerkin spectral methods with a trunkation of $N$ is equal in accuracy the corresponding pseudospectral method with a trunkation of $(N + 1)$ or $(N + 2)$ [6].

When solving the equations modeling the convection cells, high accuracy is important, and both the Galerkin spectral and the pseudospectral methods provide good accuracy for moderately low values of $N$. A concern with the pseudospectral methods is that the resulting matrix is full, which gives higher computation time. However, in test runs on a two-dimensional inhomogeneous heat equation, the Galerkin spectral methods turned out to be slower than the pseudospectral methods owing to the numerical integration. Since the pseudospectral methods still have the advantage of easy implementation of complex boundary conditions, pseudospectral methods is preferred in our case.

## 6.2 Pseudospectral Methods

Pseudospectral methods are closely related to finite differences, and showing this relationship can illustrate why pseudospectral methods have such good convergence properties. The two methods are based on grid points; while the Galerkin spectral methods find a linear combination of functions that approximates the solution in the whole domain, both the pseudospectral methods and the FDM base on finding approximate values in some specific

points and afterwards interpolation between these points are needed to find the complete solution. This similarity allows us to compare the data structure of FDM and the pseudospectral methods.

The FDM finds a difference expression between some of the grid points in order to mimic the behaviour of derivatives. For example, on an evenly spaced grid with node distance $h$, the derivative in an interior point may be approximated by the three-point formula

$$\frac{df}{dx}(x_i) = \frac{f(x_{i+1}) - f(x_{i-1})}{2h} + O(h^2).$$

This formula is a second order formula since the error acts as $h^2$ when $h \to 0$. Higher order methods are achieved if information from several points are used. For a first order one-dimensional ODE, a FDM approach using the above difference expression, yields a linear system consisting of a tridiagonal matrix. Since the pseudospectral methods are built in a similar manner as the FDM, and the resulting matrix $\mathbf{A}$ is full, it follows that the pseudospectral differentiation expressions can be interpreted as $(N+1)$-point formulas. If the solution is smooth enough, we expect the error to be $O(h^N)$ as $h \to 0$. Since the node distance $h$ is of order $1/N$, this gives an expected convergence rate of $O(1/N^N)$ as $N \to \infty$. A more thorough convergence analysis of the pseudospectral methods will be given in Section 6.4.

### 6.2.1 Choice of Basis Functions and Collocation Nodes

When working with spectral methods, the choice of basis functions is very important since the wrong choice of basis functions may give poor convergence properties or, in a worst case scenario, create a discretization that will not converge to the correct solution at all. Obvisously, the basis functions need some basic properties. We need them to be easy to compute, rapidly converging and complete. In this context, "complete" means that any solution can be represented to arbitrarily high accuracy by making $N$ sufficiently large [6].

Boyd introduces a "moral principle" on how to choose the basis functions, see Figure 6.1.

We need one choice of basis functions for each of the three dimensions $r$, $\theta$ and $z$. For the radial and vertical directions, we will use Chebyshev polynomials as basis, while in azimuthal direction we have $2\pi$-periodicity and choose Fourier series.

**MORAL PRINCIPLE 1:**

*(i) When in doubt, use Chebyshev polynomials unless the solution is spatially periodic, in which case an ordinary Fourier series is better.*

*(ii) Unless you're sure another set of basis functions is better, use Chebyshev polynomials.*

*(iii) Unless you're really, really sure that another set of basis functions is better, use Chebyshev polynomials.*

Figure 6.1: Borrowed from page 10 in [6].

After choosing the appropriate basis functions, we need to choose the actual collocation nodes and corresponding cardinal functions. In radial and vertical direction we will use a $(N+1)$ Gauss-Lobatto-Chebyshev[2] (GLC) grid, which consists of the critical points of the $N$th order Chebyshev polynomial $T_N(x)$, and the endpoints $-1$ and 1, as seen in Figure 6.2. These points are easily shifted and scaled to fit into the two intervals $[R_w, R]$ and $[0, 1]$.

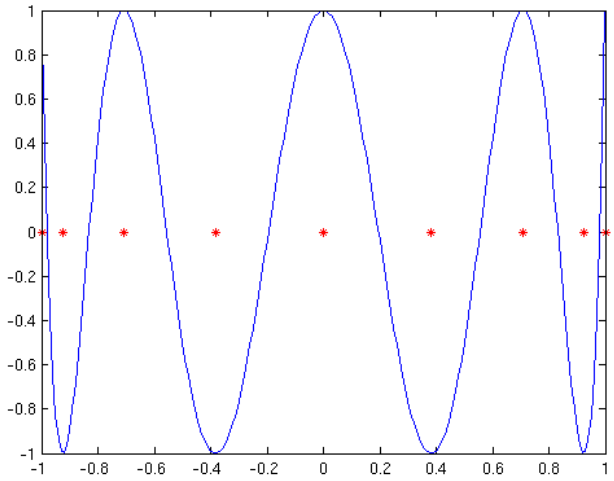


Figure 6.2: GLC grid for $N = 8$. The blue line is the Chebyshev polynomial $T_8$, while the red dots are the endpoints and the critical points of $T_8$.

[2]Another possible grid when using Chebyshev basis, is the Gauss-Radau-Chebyshev grid. It is rarely used as grid in pseudospectral methods and will not be considered in this thesis.

The $(N+1)$ GLC points are given by

$$x_i = \cos\left(\frac{\pi i}{N}\right) \text{ for } i = 0, \ldots, N, \tag{6.7}$$

while the cardinal functions satisfying the kronecker-delta property (6.6) will be given by

$$C_i(x) = \frac{(-1)^{i+1}}{c_i N^2} \frac{(1-x^2)}{(x-x_i)} \frac{dT_N(x)}{dx} \tag{6.8}$$

where $c_i$ is 2 when $i$ is 0 or $N$ (corresponding to the endpoints) and otherwise 1. An example of a cardinal function can be seen in Figure 6.3.

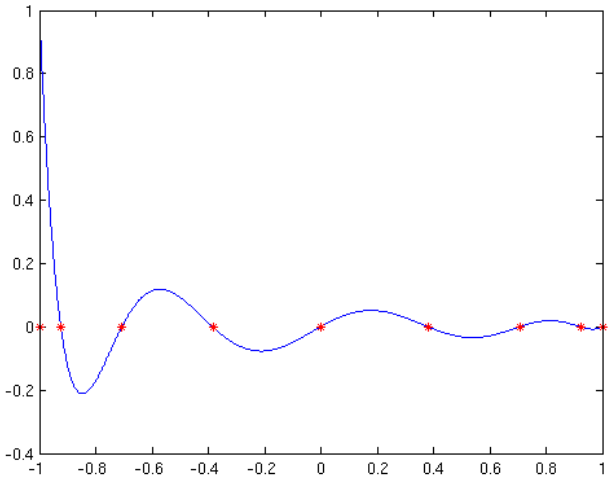


Figure 6.3: Chebyshev cardinal function corresponding to $x = -1$ when $N = 8$.

In the azimuthal direction, we use the standard grid associated with Fourier series; that is, the critical points of $\cos(Nx/2)$,

$$x_i = \frac{2\pi i}{N} \text{ for } i = 1, \ldots, N. \tag{6.9}$$

Note that we only need $N$ points in stead of $(N+1)$ points. This is due to the periodicity in the solution. The point corresponding to $i = 0$ is the same point as the one corresponding to $i = N$. Hence, $i = 0$ is neglected. The cardinal functions associated with these points are

$$C_i(x) = \frac{1}{2N} \sin\Big[N(x-x_i)\Big] \cot\Big[\frac{1}{2}(x-x_i)\Big], \tag{6.10}$$

An example of a cardinal function can be seen in Figure 6.4.

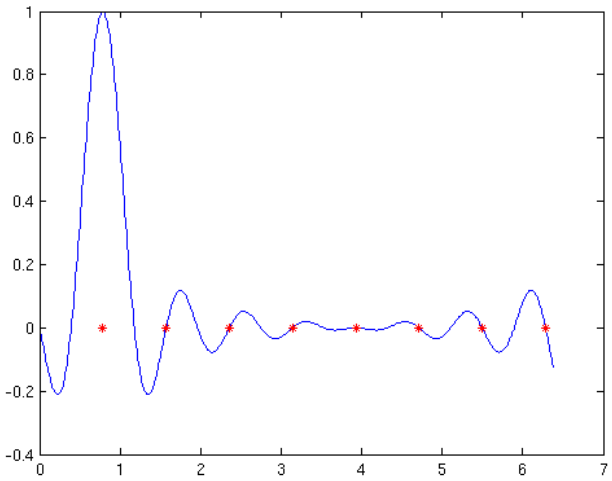


Figure 6.4: Fourier cardinal function corresponding to $x = \frac{2\pi}{N}$ when $N = 8$.

Using Chebyshev nodes in radial and vertical direction, and Fourier nodes in azimuthal direction, our resulting grid will be as seen in Figure 6.5.

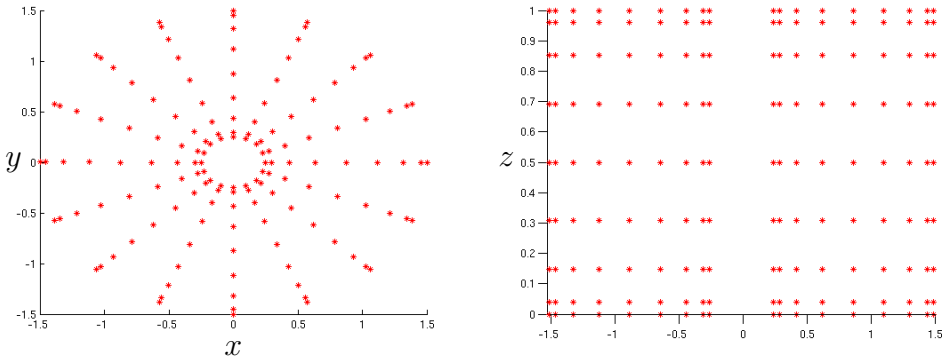


(a) Grid seen from above

(b) Grid seen from the side

Figure 6.5: Example grid with 9 points in radial and vertical direction, and 16 points in azimuthal direction.

### 6.2.2 Differentiation Matrices

As mentioned in the outline of pseudospectral methods, the resulting linear system will have a matrix with entries

$$A_{ij} = LC_j(x_i) \tag{6.11}$$

where $L$ is the differential operator. Our differential equations found in chapter 3, (3.5)-(3.7), involves both first and second order derivatives, hence we need to find matrices corresponding to first and second order derivatives to build the resulting matrix system with.

If our differential equation consisted of only a first order derivative, $\frac{du}{dx} = f$, then the resulting matrix will have entries $C_{j,x}(x_i)$, where the subscript $x$ means differentiation with respect to $x$. If the differential equation was $\frac{d^2u}{dx^2}$, the resulting matrix would have entries given by $C_{j,xx}(x_i)$. In other words, we need to find the two first derivatives of our cardinal functions (6.8) and (6.10), and evaluate them in the collocation nodes. The formulas presented in the following was found by Gottlieb, Hussaini and Orszag and given in [11].

The first derivative of the Chebyshev cardinal function (6.8) evaluated in the collocation nodes results in the differentiation matrix

$$(A_1)_{ij} = \begin{cases} (1+2N^2)/6 & \text{if } i = j = 0 \\ -(1+2N^2)/6 & \text{if } i = j = N \\ -x_j/[2(1-x_j^2)] & \text{if } i = j;\ 0 < j < N \\ (-1)^{i+j} c_i/[c_j(x_i - x_j)] & \text{if } i \neq j. \end{cases} \tag{6.12}$$

All higher order derivatives of the Chebyshev cardinal functions evaluated in the same points, hence, all higher order differentiation matrices, will be given as

$$\mathbf{A}_k = (\mathbf{A}_1)^k. \tag{6.13}$$

That is, the $k$th derivative of a function expanded with Chebyshev cardinal functions as basis, will be the same as applying the first derivative $k$ times.

The first derivative of the Fourier cardinal functions (6.10) evaluated in the collocation nodes results in the differentiation matrix

$$(A_1)_{ij} = \begin{cases} 0 & \text{if } i = j \\ 0.5(-1)^{i-j} \cot[0.5(x_i - x_j)] & \text{if } i \neq j, \end{cases} \tag{6.14}$$

while the second derivative is given by

$$(A_2)_{ij} = \begin{cases} -(1+2N^2)/6 & \text{if } i = j \\ 0.5(-1)^{i-j+1} \csc^2[0.5(x_i - x_j)] & \text{if } i \neq j. \end{cases} \tag{6.15}$$

The differentiation matrices for the three-dimensional equations are now built by creating them first for the 1D-case using the formulas (6.12)-(6.15), and then applying Kronecker tensor products to extend the matrices to three spatial dimensions. The Laplace operator is created by summing the extended second order differentiation matrices for each spatial dimension.

### 6.2.3 Boundary Conditions

The method sketched above for making the differentiation matrices does not take account of the boundary conditions (3.8)-(3.13). We will encounter two types of boundary conditions: Dirichlet conditions which assign a specific value to the unknown solution on the boundary, and Neumann conditions which specify the value of the solution's derivative on the boundary. Both Dirichlet and Neumann conditions are easily handled through the differentiation matrices.

#### Dirichlet Conditions

A representative example of a Dirichlet condition we will be using, is of the form $u = f_R(\theta, z)$ on $r = R$, which means that we assign the values $f_R(\theta, z)$ to our unknown $u$ at the outer radius $R$. To apply the boundary condition, we localize the lines corresponding to the outer radius in the matrix equation, and replace the matrix lines with zeros everywhere except at the diagonal element which is set to 1. The right-hand side of the matrix equation is assigned the corresponding value of $f_R$. The process is similar when applying Dirichlet conditions to the other boundaries.

#### Neumann Conditions

We will only encounter the homogeneous Neumann condition $\frac{\partial T}{\partial r} = 0$ at $r = R_w$ and $r = R$, but the process is similar for inhomogeneous conditions. When applying a Neumann condition, the only difference from the Dirichlet case is what you replace in the corresponding matrix lines. After localizing a line corresponding to the outer radius (as an example), the matrix elements on that line representing the other radial points of same $z$- and $\theta$-coordinate,

must be found. These elements should be replaced with the corresponding matrix elements from the discretization of $\frac{\partial}{\partial r}$ found earlier, while all other elements on the line are set to zero. Owing to the homogeneity, the corresponding element of the right-hand of the matrix equation is set to zero. The process is repeated for all lines in the matrix equation representing the outer radius. The process is similar for the Neumann condition on the inner radius.

## 6.3 Time Discretization

When the spatial dimensions are readily discretized we have a resulting ODE-system, which may be solved using one of MATLAB's own ODE-solvers. However, since we don't have a time derivative in the matrix lines where we applied boundary conditions, we have a system of differential-algebraic equations (DAE-system), and not a pure ODE-system. We therefore use the MATLAB solver ODE15s, which can handle DAE-systems.

ODE15s is an adaptive solver using quasi-constant step sizes based on the backward differentiation formulas up to a maximum order five. The time-stepper handles non-linearities in the input function through a simplified Newton iteration by approximating and reusing the Jacobian of the system of equations. ODE15s behaves very well with nonstiff problems, but is also suitable for stiff problems. However, the accuracy of ODE15s is only low to medium [26].

Technical details on the implementation of the pseudospectral methods and connecting the spatial discretization with ODE15s is given in Appendix B.

## 6.4 Convergence of Pseudospectral Methods

As stated earlier, we expect the convergence rate of pseudospectral methods to be $O(1/N^N)$. The rapid convergence rate of spectral methods owe to the convergence properties of series expansions of orthogonal functions.

When solving a PDE using pseudospectral methods, there are several sources of error. Boyd [6] separates between

- Truncation error: the truncation error is defined to be the error made by neglecting all spectral coefficients $a_j$ with $j > N$ of the solution's series expansion (or translated to pseudospectral's terminology: the

error made by only using $(N+1)$ collocation points and not infinitely many[3]).

- Discretization error: the discretization error is the difference between the first $(N+1)$ terms of the series expansion of the exact solution and the corresponding terms computed by pseudospectral methods.
- Interpolation error: the interpolation error is the error made by approximating a function by a $(N+1)$-term series whose coefficients are chosen to make the approximation agree with the target function exactly at $(N+1)$ interpolation/collocation points.

It is generally impossible to determine these various errors precisely. As the exact solution is unknown, we do not have control over any of the errors. However, the truncation error may be estimated by computing the expansion of a known function that is believed to act in a similar manner as the exact solution. Furthermore, Boyd argue that through many years of numerical experience one can justify the assumption that the discretization and interpolation errors are the same order of magnitude as the truncation error. Therefore, one can roughly estimate the accuracy of pseudospectral methods by inspecting the (estimated) truncation error alone.

In order to estimate the truncation error, we take a closer look upon convergence properties of Fourier and Chebyshev series. The teory presented here is based on the book of Gottlieb and Orszag [12].

### 6.4.1 Fourier Series

The complex Fourier series of a known function $f(x)$ defined on the interval $[0, 2\pi]$ is the periodic function

$$g(x) = \sum_{j=-\infty}^{\infty} a_j e^{ijx},$$

where $i$ now refers to the complex number $\sqrt{-1}$ and where the series coeffiecient $a_j$ are given by

$$a_j = \frac{1}{2\pi} \int_0^{2\pi} f(x) e^{-ijx} \mathrm{dx}.$$

[3]It may not be obvious why these two "definitions" of the truncation error is the same, but as Boyd shows, the Galerkin approach through a series expansion is equivalent with the pseudospectral approach through collocation points if the collocation points are quadrature points in a Gaussian quadrature rule. For more details, see chapter 4.4 in [6].

If we define $g_N(x)$ as the truncated series

$$g_N(x) = \sum_{j=-N}^{N} a_j e^{ijx},$$

we wish to estimate the convergence rate of $|f(x) - g_N(x)|$ as $N \to \infty$. If $f(x)$ is periodic, and has continuous derivatives up to order $(k-1)$ for some positive integer $k$, and if $f^{(k)}(x)$ is integrable, then integration by parts yields

$$a_j = \frac{1}{2\pi(ij)^k} \int_0^{2\pi} f^{(k)}(x) e^{-ijx} \mathrm{dx}.$$

Since $f^{(k)}$ is integrable, the Riemann-Lebesgue lemma implies that $a_j \ll 1/j^k$ when $j \to \pm\infty$. It is possible to show that if $a_j$ goes to zero like $1/j^k$ and no faster, then the error is

$$g_N(x) - f(x) = O\Big(\frac{1}{N^k}\Big) \text{ as } N \to \infty,$$

which is called algebraic convergence of order $k$. In particular, if $f(x)$ is infinitely differentiable and periodic, then

$$g_N(x) - f(x) = O\Big(\frac{1}{N^k}\Big) \ \forall k \geq 0 \text{ as } N \to \infty, \tag{6.16}$$

which means that $g_N(x)$ converges to $f(x)$ more rapidly than any finite power of $1/N$ as $N \to \infty$. This order of convergence is called exponential or spectral convergence.

### 6.4.2 Chebyshev Series

The convergence theory for Chebyshev series is similar to that of Fourier cosine series since the Chebyshev series is just a disguised Fourier cosine series: When a function $f(x)$ defined on the interval $[-1, 1]$ has a Chebyshev series given by

$$g(x) = \sum_{j=0}^{\infty} a_j T_j(x),$$

then $G(\theta) = g(\cos\theta)$ is the Fourier cosine series of $F(\theta) = f(\cos\theta)$ for $\theta \in [0, \pi]$. This follows directly from the cosinus-property of Chebyshev polynomials; that is, $T_j(\cos\theta) = \cos(j\theta)$, and using the mapping $x = \cos\theta$. The series coefficients $a_j$ in the Chebyshev series will be given by

$$a_j = \frac{2}{\pi d_j} \int_0^{\pi} f(\cos\theta)\cos(j\theta)\mathrm{d}\theta = \frac{2}{\pi d_j} \int_{-1}^{1} f(x) T_j(x)(1-x^2)^{-1/2}\mathrm{dx},$$

where $d_0 = 2$ and otherwise 1. Since a Fourier cosine series has the same convergence properties as a normal Fourier series when applicable, the Chebyshev series will also have the same convergence properties. Hence, if $f(x)$ is infinitely differentiable[4], the truncated series expansion $g_N(x) = \sum_{j=0}^{N} a_j T_j(x)$ converges to $f(x)$ at exponential/spectral rate as $N \to \infty$.

However, it is important to note that for both Fourier and Chebyshev discretizations, spectral convergence is only obtained when the unknown solution has infinitely many continuous derivatives. This assumption is usually too optimistic.

[4]Periodicity in the function $f(x)$ is not necessery when using Chebyshev series since the coordinate transform $x = \cos\theta$ assures $2\pi$-periodicity independently of $f$.

# Chapter 7

# Results and Discussion - Simulations

The unsteady simulator built using pseudospectral methods and ODE15s, solve the governing nonlinear equations (3.5)-(3.7). The simulator's input is the dimensions of the cylinder, the Rayleigh number and vertical boundary conditions, and the output is the temperature distribution and velocity field after a certain amount of time. From the temperature distribution and velocity field, we are enabled to determine the convection pattern, hence we can investigate how the nonlinear regime differs from that of the linearized system. The solver may also be used to examine the stability of existing convection cells: Through simulations we may investigate the effect of variations in the Rayleigh number and find out how a specific convective mode responds when the domain changes or when a numerical perturbation is added during a simulation. At last we attempt to investigate the effect of convection cells on heat fluxes into a heat producing well.

## 7.1 Comparison with Linear Results

In Chapter 5, we found critical Rayleigh numbers and corresponding mode maps using a linear stability analysis. However, linearizing the equations raises the question if we made severe errors through the linearization. There is a possibility that our assumption of *small* temperature variations is not valid in the original nonlinear equations, hence making our estimates for the critical Rayleigh numbers and mode maps useless for real-world applications. Using the unsteady simulator to solve the governing, nonlinear equations and compare the appearing mode with the one found using linear analysis, enables us to determine the validity of the linear analysis.

Furthermore, the linear analysis is not able to say anything about stability and appearence of the (higher order) modes, nor how the Rayleigh number affects the convection. These questions can also be answered through simulations.

### 7.1.1 Critical Rayleigh Numbers

For both the conducting and insulated sidewalls, simulations provided approximately the same estimates for the critical Rayleigh number as the linear analysis. Steady solutions involving convection cells were obtained for different values of Ra above the critical value given by linear theory. Weakly nonlinear theory for systems in which supercritical bifurcations occur indicate that the amplitude of convection is proportional to $(\mathrm{Ra} - \mathrm{Ra}_c)^{1/2}$, meaning that the square of the amplitude will be proportional to $(\mathrm{Ra} - \mathrm{Ra}_c)$. Thus we may extrapolate backwards to determine the critical value of Ra from the point of view of the nonlinear code. In our context, the amplitude is given by

$$A = \sqrt{\Big[\int_V T\sin(m\theta)\mathrm{dV}\Big]^2 + \Big[\int_V T\cos(m\theta)\mathrm{dV}\Big]^2},$$

where the integrals are taken over the volume of the annular cylinder. Values of $\mathrm{Ra}_c$ obtained in this way were compared with the analytical solutions and were found to compare well, thereby lending confidence to the accuracy of the numerical coding and the quality of the numerical results.

Starting out with the Rayleigh number being larger than the critical, hence obtaining a stable convection pattern, and then gradually lowering the Rayleigh number below the critical, always resulted in the convection pattern decreasing in magnitude before disappearing completely when the critical Rayleigh number predicted from the linear stability analysis was reached.

### 7.1.2 Mode Maps

Simulations with Rayleigh number slightly larger than the critical in order to test which convective mode appeared, generally provided the convection mode predicted from the above analysis. The linear regime is therefore adequate for describing the convection pattern in the nonlinear regime for Rayleigh number slightly above the critical. However, for the conducting sidewalls, simulations provided the correct value of $m$, but when the linear

analysis predicted $p$ to be 4 or larger in the heat conducting sidewalls case, simulations always provided a smaller value of $p$. The reason for this is either that our solver is not able to reproduce convective modes with large values of $p$ when the sidewalls are heat conducting, or that the linear analysis is not suitable for describing the nonlinear regime in these cases.

As mentioned in Section 5.2.2, our mode map is not entirely equal to the one obtained by Bau and Torrance [2]. Simulations with the inner and outer radius chosen corresponding to the positions in the mode maps where deviations were present, resulted in the mode predicted from our mode map.

### 7.1.3 Higher Order Modes

Simulations with Rayleigh numbers slightly larger than $\mathrm{Ra}_{c,n}$, for some positive integer $n$, could both produce the basic mode $(m, p)$, but also higher order modes up to $(m_n, p_n)$ appeared. A detailed comparison would have to be made with a weakly nonlinear analysis of the respective modes and their interaction, rather than with the linearized theory, and this aspect is outside of the scope of this master thesis. However, Riley and Winters [27] made a very thorough study of the modal exchange mechanisms for convection in a two dimensional porous cavity using a stationary finite element solver coupled with bifurcation tracking software. In that paper they showed that the second mode that appears is generally unstable but eventually gains stability as Ra increases.

The scenario of Riley and Winters also applies in the present three-dimensional context, as may be seen in Figure 7.1. Here we show a case with insulated sidewalls where $R_w = 0.1$ and $R = 0.7$. The critical Rayleigh numbers for the first two modes, $(1, 0)$ and $(2, 0)$, are 41.41 and 43.82. The $(1, 0)$ remains stable with respect to numerical perturbations within the range of values of Ra we consider, but the $(2, 0)$ mode is only stable above $\mathrm{Ra} = 50$. The secondary mode becomes unstable for lower Rayleigh numbers since this mode should disappear for a Rayleigh number larger than the (basic) critical, hence the basic mode will take over when the secondary is in the process of disapperaing since convection is still possible. Since the different modes have overlapping stability regions; hence, several modes are possible for a given Rayleigh number. We cannot speak of a *preferred* mode since which mode to appear depends on the initial conditions.

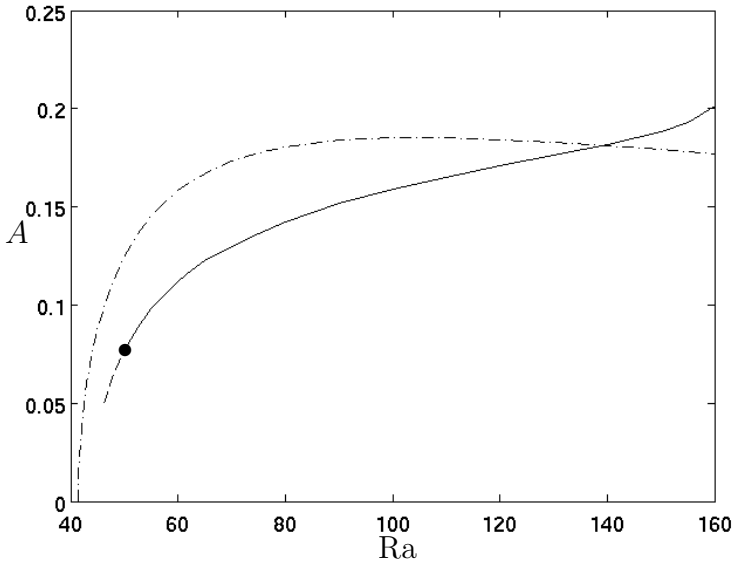


Figure 7.1: The variation of the amplitude of convection with Rayleigh number for modes $(1,0)$ and $(2,0)$ for $R_w = 0.1$ and $R = 0.7$ and with insulated sidewalls. The dashed/dotted line is the amplitude of the basic mode $(1,0)$. The continuous line is the amplitude of the stable part of the secondary mode $(2,0)$ branch, while the dashed line is the unstable part. Our solver was not able to extend the dashed line any further owing to numerical instabilities.

### 7.1.4 The Appearence of Mixed Modes

In the insulated sidewalls case, stable modes not present in the linear analysis was found. For values of the outer radius larger than 1, convective modes being intermediate of two other modes, so-called mixed modes, could be found. For example, for $R_w = 0.7$ and $R = 2.1$, the first and secondary modes are $(5,0)$ and $(2,1)$. The critical Rayleigh numbers corresponding to these patterns are 39.51 and 39.58. When Ra $= 39.75$ the stable solution shown in Figure 7.2 arises. It is clear from the Figure that an $m = 2$ pattern dominates near the inner radius and an $m = 5$ pattern dominates near the outer radius.

The amplitude and stability regions for the mode $(5,0)$ and the mixed mode are sketched for low Rayleigh numbers in Figure 7.3. This Figure suggests that the mixed mode bifurcates away from the pure mode, rendering the latter unstable. The secondary mode $(2,1)$ is unstable for all low Rayleigh

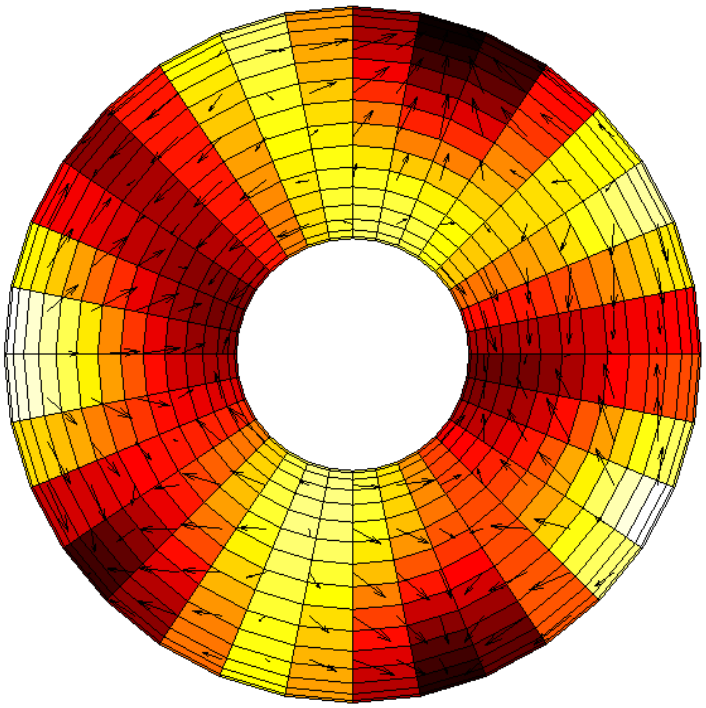

Figure 7.2: The convection mode has $m = 2$ near the inner radius, while $m = 5$ near the outer radius. The value of $p$ is either 0 or 1 depending on which radial ray you look at.

numbers, hence this mode is not present in the Figure.

These mixed modes would be impossible to detect by the linear stability analysis, since the solution of the linearized equations only allow one value of $m$ and $p$ describing the convection in the whole domain. Hence, these intermediate modes develop owing to nonlinear effects. The mixed modes were only observed for outer radius larger than 1, possibly because of the severe clustering of modes present for larger outer radius. We also observed that for even larger outer radius, the mixed modes became more dominating over the basic mode; that is, the basic mode had a smaller stability region. It is likely to believe this effect to be even more important when the outer radius increase further, hence the classical approach of assigning *one* value of $m$ and $p$ to describe the convection patterns will not be sufficient.

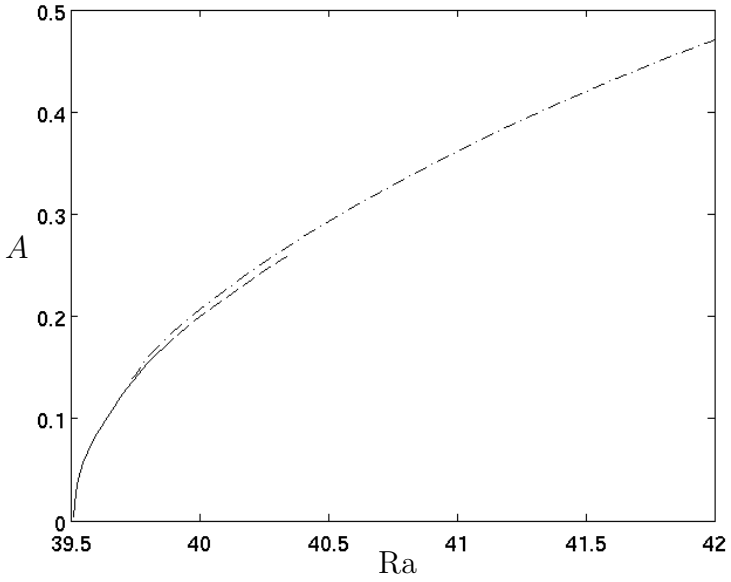


Figure 7.3: The variation in amplitude of convection with Ra for the case $R_w = 0.7$ and $R = 2.1$, with insulated sidewalls. The continuous line corresponds to the stable part of the basic mode $(5, 0)$ having critical Rayleigh number 39.51, while the dashed line is the unstable region of this mode. The dashed-dotted line is the stable mixed mode branch.

## 7.2 Stability of Convection Cells

As already mentioned above, we have considered the stability with respect to numerical perturbations. Also, stability with respect to perturbations in the domain was investigated.

### 7.2.1 Stability with Respect to Numerical Perturbations

In order to investigate the convection cells' stability with respect to perturbations, numerical perturbations of different magnitudes was added to a stable convection mode and then timestepped until stability again was reached. Adding random perturbations of magnitudes from $10^{-6}$ to $10^{-1}$ resulted in the perturbations dying out quickly if in a stability region, but would give a different mode if outside the mode's stability region (cf Figures 7.1 and 7.3).

Two different convective modes can have overlapping stability regions until the point where the recessive mode becomes unstable. We observed two

different cases of this phenomena: In the first case, as captured in Figure 7.1, the basic mode is stable for all (observable) Rayleigh numbers larger than the critical, while the second order mode becomes unstable when the Rayleigh number approach $\mathrm{Ra}_{c,2}$. The second order mode is recessive for smaller Rayleigh numbers: In the case investigated in the figure, $\mathrm{Ra}_{c,2}$ was 43.82, hence the solid line should in theory approach zero for this Rayleigh number. However, convection is possible for all Rayleigh numbers larger than the first critical Rayleigh number, so when the second order mode is in the process of disappearing, the basic mode will take over, hence making the second order mode unstable.

The other appearence of modes becoming recessive, is in the appearence of mixed modes and is observed in Figure 7.3. Here, the basic mode is unstable for larger Rayleigh numbers because of the dominance of the mixed mode.

### 7.2.2 Stability with Respect to the Domain - Sharpness of Bifurcation Trajectories

Simulations can reveal if bifurcation trajectories from the mode maps are equally sharp and present in the nonlinear case by choosing values of $R_w$ and $R$ close to each other and at each side of a bifurcation trajectory, and with Rayleigh number slightly over the critical. In both the insulated and the conducting sidewalls case, the bifurcation trajectories from the mode maps were found to be present at the positions given by the linear analysis (with the exceptions for bifurcation trajectories concerning $p$ larger than 4 for the conducting sidewalls). Choosing values of the inner and outer radius less than 0.005 nondimensional length units away from a bifurcation trajectory, provided a mixed mode at onset, but the mode stabilized at the mode predicted from the linear analysis when using low Rayleigh numbers.

However, given a convection mode near a bifurcation trajectory, and perturbing the domain such that another convection mode should be the preferred according to the analysis, produced this other mode. Hence the convection modes are not stable with respect to domain perturbations near the bifurcation trajectories. We may also conclude that the bifurcation trajectories are sharp; there are no transition zones. The mode at the other side of the trajectory will, however, appear as a secondary mode, with stability properties as described above.

Even though mixed modes could appear at onset this does not contradict

the conclusion that the bifurcation trajectories are sharp since these mixed modes were not stable.

## 7.3 Experiment: Heat Fluxes into a Heat Producing Well

To investigate the effect of convection cells on heat fluxes in a porous medium, we have designed some preliminary experiments. We apply our simulator to an experiment involving three cases, and compare heat fluxes into the heat producing well. The experiment concerns the annular cylinder with heat conducting sidewalls where the inner cylinder represents a closed and heat producing well, and the outer cylinder having a radius of 4 represents the end of a large heat reservoir which were assumed to be kept at the linear temperature used earlier. The inner cylinder has a radius of $10^{-6}$ and is cooled to various linear temperature distributions in order to observe the effect of a cooled well. Schematically, the experiment setup is as illustrated in Figure 7.4.

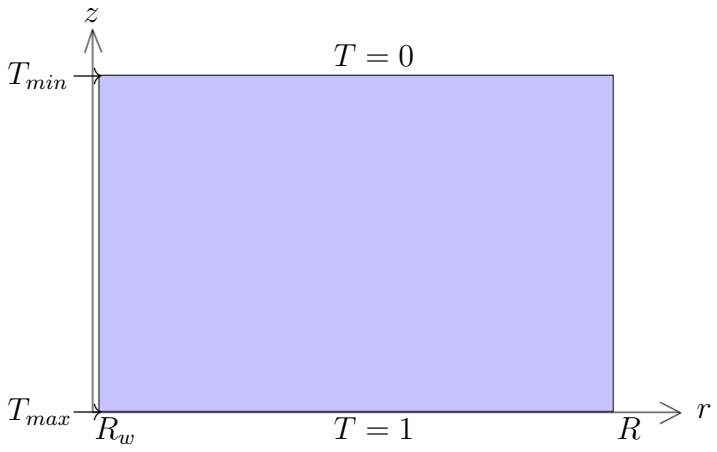


Figure 7.4: The inner radius is kept at a linear temperature distribution where $T = T_{max}$ at $z = 0$ and $T = T_{min}$ at $z = 1$. We still apply $T = 1 - z$ at the outer radius, and the top and bottom of the cylinder are as always kept at $T = 0$ and $T = 1$, respectively.

The well is kept at the linear temperature distribution given by

$$T = T_{max} - (T_{max} - T_{min})z, \tag{7.1}$$

where $T_{max}$ is allowed to vary between 0 and 1, and $T_{min}$ may vary between $(-1)$ and 0. Note that a negative temperature in our nondimensional variables only means that the temperature is lower than the temperature of the cylinder's top.

We consider three different cases:

**Case I** Rayleigh number 45 (that is, larger than the critical if no cooling of the well),

**Case II** Rayleigh number 35 (that is, smaller than the critical if no cooling of the well),

**Case III** No convection allowed; all velocities are set to zero.[1]

Case II will still provide convection due to the cooling of the well. Hence convection cells are expected to be present in Case I and II, but the convection should be stronger in Case I.

For each of the three different cases, we timestep the simulator until stability is reached and then calculate the total (nondimensional) heat flux $Q_w$ into the well, which is given by

$$Q_w = -\int_{\delta R_w} \nabla T \cdot \mathbf{n} \mathrm{dS}.$$

The integral is taken over the vertical boundary of the well, and $\mathbf{n}$ is the outward unit vector of the well. Since $\mathbf{n} = \mathbf{e_r}$, that is, the radial unit vector, then

$$\nabla T \cdot \mathbf{n} = \frac{\partial T}{\partial r}.$$

### 7.3.1 Results for the Three Different Cases

Varying $T_{max}$ and $T_{min}$ and calculating the corresponding heat fluxes into the well, produces the heat fluxes given in Table 7.1. Note that even though we observe equal values of the heat fluxes for different degrees of cooling in Table 7.1(c), the temperature distributions in the porous medium are not equal.

From Table 7.1 we see the expected tendency that a cooler well provides a larger heat flux into the well. However, the convection cells have a negative

[1] This case corresponds to only solving the heat equation since the convective term in the energy equation (3.7) disappears.

(a) Case I

| $T_{min}\backslash T_{max}$ | 0 | 0.25 | 0.5 | 0.75 | 1 |
|---|---|---|---|---|---|
| -1 | 73.72 | 61.45 | 49.43 | 37.74 | 26.39 |
| -0.75 | 62.59 | 50.53 | 38.79 | 27.53 | 16.99 |
| -0.5 | 51.72 | 39.43 | 28.79 | 18.19 | 9.02 |
| -0.25 | 41.29 | 30.24 | 19.38 | 10.38 | 2.34 |
| 0 | 30.53 | 19.76 | 10.52 | 2.48 | 0 |

(b) Case II

| $T_{min}\backslash T_{max}$ | 0 | 0.25 | 0.5 | 0.75 | 1 |
|---|---|---|---|---|---|
| -1 | 79.43 | 67.81 | 56.50 | 45.56 | 35.07 |
| -0.75 | 68.85 | 57.48 | 46.47 | 35.90 | 25.86 |
| -0.5 | 58.47 | 47.39 | 36.73 | 26.57 | 17.64 |
| -0.25 | 48.30 | 37.55 | 27.27 | 17.57 | 8.50 |
| 0 | 38.31 | 27.96 | 18.09 | 8.80 | 0 |

(c) Case III

| $T_{min}\backslash T_{max}$ | 0 | 0.25 | 0.5 | 0.75 | 1 |
|---|---|---|---|---|---|
| -1 | 96.54 | 84.47 | 72.41 | 60.34 | 48.27 |
| -0.75 | 84.47 | 72.41 | 60.34 | 48.27 | 36.20 |
| -0.5 | 72.41 | 60.34 | 48.27 | 36.20 | 24.14 |
| -0.25 | 60.34 | 48.27 | 36.20 | 24.14 | 12.07 |
| 0 | 48.27 | 36.20 | 24.14 | 12.07 | 0 |

Table 7.1: Heat fluxes into cooled well.

effect on the heat fluxes; equal degree of cooling provides a smaller heat flux into the well when convection is present. This negative effect is caused by the distribution of the convection cells near the well; the cooled well triggers a toroidal convection cell stretching around the well and has the flow direction observed in Figure 7.5(a). This flow direction causes cold fluid flowing down along the well and hot fluid flowing upwards away from the well. Hence the radial temperature gradient near the well is smaller, giving a smaller heat flux into the well in Case I and Case II, see Figure 7.5.

### 7.3.2 Alternative Approaches to Determine the Effect of Convection Cells

The above experiment has its main limitation in the unrealistic boundary conditions at the top and bottom of the annular cylinder. Keeping the top and bottom at constant temperatures corresponds to assuming there beeing

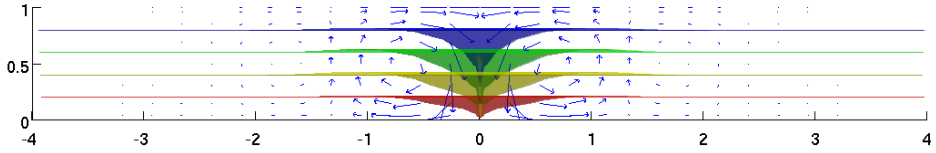


(a) Case II

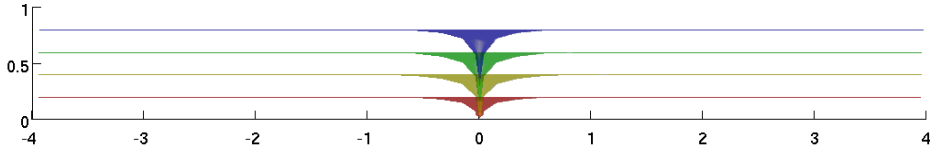


(b) Case III

Figure 7.5: Temperature distribution near the well when the inner radius is cooled such that $T_{min} = -0.5$ and $T_{max} = 0.5$. The red, yellow, green and blue surfaces represents temperatures of 0.8, 0.6, 0.4 and 0.2, respectively.

an infinite heat reservoir below the porous medium and an infinite heat receiver above it. More realistic would be to model the rock below and above the porous medium. A possible approach would be to model the three-layered domain sketched in Figure 7.6.

Further investigation of the effect of convection cells could be to allow the well to be permeable in the porous layer of Figure 7.6; representing injection and production of fluid. Injecting and producing fluid in different heights of the layer could trigger the convection cells to distribute in a manner resulting in a larger heat production. Also, modelling the well explicitly in stead of only as a boundary condition for the annular cylinder, would enable us to provide more realistic boundary conditions on the well. Other possible additions would be to model the temperature in the solid and in the fluid separately to get a more realistic temperature distribution. However, all the above mentioned modifications of the model would require making significant changes to the simulator, which is beyond the scope of this master thesis.

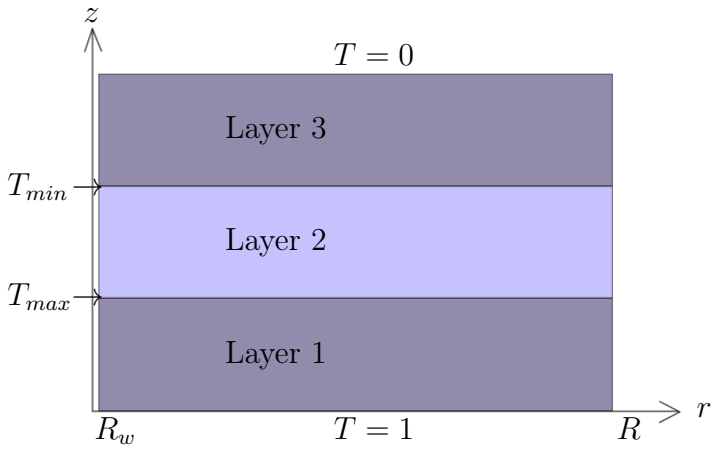


Figure 7.6: Layers 1 and 3 are assumed impermeable, but are able to conduct heat. Layer 2 is the porous medium. The inner radius is assumed insulated in layers 1 and 3.

# Chapter 8

# Summary and Conclusions

In this thesis we have developed a model for convection cells in a porous cavity between two vertical coaxial cylinders that are heated from below and cooled from above. The model equations needed to describe the convection cells under our assumptions were presented in Chapter 2 and transformed to nondimensional form in Chapter 3. We applied a linear stability analysis to the resulting model in Chapter 4 and were able to find an analytical solution to the linear equations through separation of variables. The analytical solution enabled us to develop a strategy for determining the critical Rayleigh number for onset of convection and finding the corresponding preferred modes as well as higher order modes.

In accordance with previous studies, we find the critical Rayleigh numbers to converge to $4\pi^2$, and always be larger for heat conducting sidewalls. Our results show that the effect of an inner radius is more severe for heat conducting sidewalls. The presence of an inner cylinder increase the critical Rayleigh number significantly compared to the non-annular cylinder studied by Haugen and Tyvand [13]. For the insulated sidewalls, the inner radius does not have a similar effect. Letting the inner radius approach zero, our results show that the problem with insulated sidewalls degenerates into the one studied by Zebib [33], while a small heat conducting inner radius would still affect the critical Rayleigh number. Letting the inner radius approach zero, the case of Haugen and Tyvand appears as a special case in our analysis.

Our linear analysis provides maps over preferred convective modes for the two cases, and in general our results show the appearance of more convection cells in radial direction for increasing outer radius, and more convection cells in azimuthal direction for increasing inner radius. For the insulated sidewalls case, we sometimes find other modes than Bau and Torrance [2]

found in their paper. High-resolution simulations confirms our analysis.

To investigate the nonlinear regime we designed a numerical solver using pseudospectral methods in Chapter 6. The aim of the numerical solver was both to determine the applicability of the linear analysis for the nonlinear regime with respect to onset of convection and preferred convective modes at onset, but also to consider the stability of the convection cells and how the nonlinear regime would behave at different Rayleigh numbers. We also planned to use the simulator with boundary conditions that would be more realistic with respect to geothermal energy extraction.

Simulations with various inner and outer radii, and with Rayleigh numbers slightly above critical, conform in most cases to the convection modes and critical Rayleigh numbers predicted from the linear analysis. Our results show that the various modes have Rayleigh number dependent stability regimes, which is an important factor in predicting the convective mode occuring in practice. The nonlinear regime also reveals the appearance of mixed modes that are not represented in the basis of the linear analysis. As such, the numerical simulations both verify the linear stability analysis, as well as give bounds on its validity.

Our experiment in Section 7.3 seemingly reveals that convection cells may have a significant effect on the heat extraction. As the horizontal boundaries were perfectly heat conducting, our findings are not realistic. Modifications to the simulator will be made to enable modelling of boundary conditions mimicking extraction of energy from a geothermal reservoir.

# Appendix A

# Separation of Variables

We wish to solve the linear equation

$$\nabla^4 \hat{T} + \mathrm{Ra}\nabla_1^2 \hat{T} = 0, \tag{A.1}$$

using separation of variables when the top and bottom walls of the cylinder are impermeable and conducting:

$$\nabla^2 \hat{T} = 0 \text{ at } z \in \{0, 1\}, \tag{A.2}$$

and

$$\hat{T} = 0 \text{ at } z \in \{0, 1\}. \tag{A.3}$$

Haugen and Tyvand [13] solve the same equation with the same two boundary conditions in $z$. They argue that at the onset of convection between horizontal planes that are impermeable and perfectly heat conducting, the relation

$$\nabla_1^2 \hat{T} = \nabla^2 \hat{T} + \pi^2 \hat{T} \tag{A.4}$$

is satisfied. This implicitly means that

$$\frac{\partial^2 \hat{T}}{\partial z^2} = -\pi^2 \hat{T}, \tag{A.5}$$

since $\nabla_1^2 = \nabla^2 - \frac{\partial^2}{\partial z^2}$.

We are using separation of variables, which means that we assume the solution $\hat{T}$ to be of the form

$$\hat{T}(r, \theta, z) = \mathcal{R}(r)\Theta(\theta)\mathcal{Z}(z). \tag{A.6}$$

Inserting (A.6) into the relationship (A.5) yields

$$\frac{d^2\mathcal{Z}}{dz^2} = -\pi^2\mathcal{Z},$$

which, together with the boundary conditions (A.3), gives

$$\mathcal{Z}(z) = \sin(\pi z). \tag{A.7}$$

This solution for $\mathcal{Z}(z)$ also satifies the other boundary condition (A.2). We need $\Theta(\theta)$ to be $2\pi$-periodic, hence any function

$$\Theta(\theta) = \cos(m\theta), \tag{A.8}$$

where $m$ is some positive integer, is possible.

To find $\mathcal{R}(r)$, we insert the relationship (A.4) into the original Equation (A.1):

$$\nabla^4\hat{T} + \mathrm{Ra}\nabla^2\hat{T} + \mathrm{Ra}\pi^2\hat{T} = 0.$$

This can be written

$$(\nabla^2 + a)(\nabla^2 + b)\hat{T} = 0, \tag{A.9}$$

where $a$ and $b$ must satisfy

$$a + b = \mathrm{Ra} \text{ and } a * b = \mathrm{Ra}\pi^2. \tag{A.10}$$

The constants $a$ and $b$ are solutions of the same quadratic equation, hence they will given by

$$a = \frac{\mathrm{Ra} + \sqrt{\mathrm{Ra}^2 - 4\pi^2\mathrm{Ra}}}{2}$$

$$b = \frac{\mathrm{Ra} - \sqrt{\mathrm{Ra}^2 - 4\pi^2\mathrm{Ra}}}{2}$$

We see that we only have real solutions when the Rayleigh number is larger than $4\pi^2$, which is reasonable since the critical Rayleigh number for an infinite porous layer with impermeable and conducting top and bottom will always be greater than or equal to $4\pi^2$. Restricting the porous medium inside an annular cylinder will only increase the critical Rayleigh number. We also observe that $a$ and $b$ will always be greater than $\pi^2$ in this case.

Using Equation (A.9), we can in stead solve the Helmholtz Equation

$$\nabla^2\hat{T} + c^2\hat{T} = 0,$$

where $c^2$ is either $a$ or $b$. We use separation of variables and insert the separation assumption (A.6) using the already found solutions for $\mathcal{Z}(z)$, (A.7), and for $\Theta(\theta)$, (A.8), resulting in

$$\frac{1}{r}\frac{d}{dr}\Big(r\frac{d\mathcal{R}}{dr}\Big)\cos(m\theta)\sin(\pi z) + \frac{1}{r^2}\mathcal{R}(-m^2)\cos(m\theta)\sin(\pi z) \\ +\mathcal{R}\cos(m\theta)(-\pi^2)\sin(\pi z) + c^2\mathcal{R}\cos(m\theta)\sin(\pi z) = 0$$

Dividing by $\cos(m\theta)\sin(\pi z)$ yields

$$\frac{d^2\mathcal{R}}{dr^2} + \frac{1}{r}\frac{d\mathcal{R}}{dr} + (c^2 - \pi^2 - \frac{m^2}{r^2})\mathcal{R} = 0 \tag{A.11}$$

which is only a modified version of Bessel's differential equation,

$$x^2\frac{d^2y}{dx^2} + x\frac{dy}{dx} + (x^2 - \alpha^2)y = 0,$$

which has solution given by Bessel functions. Our equation (A.11) therefore has the two solutions

$$\mathcal{R}(r) = J_m(r\sqrt{c^2 - \pi^2}) \text{ and } \mathcal{R}(r) = Y_m(r\sqrt{c^2 - \pi^2}),$$

where $J_m$ and $Y_m$ are the Bessel functions of order $m$ and of first and second kind, respectively.

Summing up, we end up with the two solutions

$$\hat{T}_1 = \Big[A_m J_m(kr) + B_m Y_m(kr)\Big]\cos(m\theta)\sin(\pi z), \tag{A.12}$$

$$\hat{T}_2 = \Big[C_m J_m(qr) + D_m Y_m(qr)\Big]\cos(m\theta)\sin(\pi z). \tag{A.13}$$

where the wavenumbers $k$ and $q$ are defined by

$$k = \sqrt{a - \pi^2} \text{ and } q = \sqrt{b - \pi^2}.$$

The two relations (A.10) are rewritten into two relations for $k$ and $q$:

$$k * q = \pi^2, \tag{A.14}$$

$$\mathrm{Ra} = k^2 + q^2 + 2\pi^2. \tag{A.15}$$

Using the first of these two relations, (A.14), we can eliminate the wavenumber $q$ from both the solution (A.13), and also from the Rayleigh relation (A.15). We then obtain the three equations given in Section 4.1.1.

# Appendix B

# Technical Details of the Solver

We here present some technical details concerning the implementation of the numerical solver. The code is divided into three main parts: first, creation of the data structure by initializing the grid and creating the differentiation matrices needed for the timestepping, followed by the initializing of the timestepping routine and the timestepping itself, and eventually, user output. A flow chart of the simulator is given at the end of the appendix.

## B.1 Initializing Grid and Matrices

The first part of the solver includes initialization of grid and matrices; an ordered grid must be made and differentiation matrices must be created.

### B.1.1 Make 3D-Grid

An ordering or enumeration of the points is needed in order to combine the three spatial dimensions. We use the Matlab command `meshgrid(th, r, z)`, where `th`, `r` and `z` are vectors of length $N_\theta$, $(N_r+1)$ and $(N_z+1)$, respectively, containing the different nodes in each dimension. The `meshgrid`-command creates an ordering of the points corresponding to

$$\begin{aligned}\mathbf{v} = [&r_1\theta_1 z_1,\ r_2\theta_1 z_1, \ldots,\ r_{N_r+1}\theta_1 z_1,\ r_1\theta_2 z_1, \ldots,\\ &\ldots,\ r_{N_r+1}\theta_{N_\theta} z_1,\ r_1\theta_1 z_2, \ldots,\ r_{N_r+1}\theta_{N_\theta} z_{N_z+1}]^T,\end{aligned} \tag{B.1}$$

where the notation $r_i\theta_j z_k$ here refers to the value of the vector $\mathbf{v}$ in the collocation node $(\mathtt{r}(i), \mathtt{th}(j), \mathtt{z}(k))$.

### B.1.2 Create Differentiation Matrices

In discretizing the equations (3.5)-(3.7) we need differentiation matrices for the three single derivatives $\frac{\partial}{\partial r}$, $\frac{1}{r}\frac{\partial}{\partial \theta}$ and $\frac{\partial}{\partial z}$. The differentiation matrices corresponding to each 1D-case is easily found using the formulas (6.12) and (6.14), while the expansion to three spatial dimensions are made using the matlab command `kron(X,Y)` which takes the Kronecker tensor product between the matrices `X` and `Y`. According to the data structure made through `meshgrid`, the differentiation matrices will be given by

$$\mathbf{Dr1\_3D} = \texttt{kron}(\texttt{eye}(\texttt{N\_th} * (\texttt{N\_z} + 1)), \mathbf{Dr1\_1D})$$

$$\mathbf{Dth1\_3D} = \texttt{kron}(\texttt{eye}(\texttt{N\_z} + 1), \texttt{kron}(\mathbf{Dth1\_1D}, \texttt{diag}(1./\texttt{r})))$$

$$\mathbf{Dz1\_3D} = \texttt{kron}(\mathbf{Dz1\_1D}, \texttt{eye}(\texttt{N\_th} * (\texttt{N\_r} + 1)))$$

The second order differentiation matrices for $\frac{1}{r}\frac{\partial}{\partial r}(r\frac{\partial}{\partial r})$, $\frac{1}{r^2}\frac{\partial^2}{\partial \theta^2}$ and $\frac{\partial^2}{\partial z^2}$ are made in a smililar manner.

### B.1.3 Apply Boundary Conditions

Applying the boundary conditions is done by first localizing the nodes corresponding to the vertical and horizontal boundaries. These nodes are easily found using Matlab's `find` function. After localizing, all matrix lines corresponding to the boundary nodes (cf the ordering of nodes given by (B.1)) are set to zero and then replaced by a discrete version of the boundary condition. For example, in the case of the insulated sidewalls, all matrix lines corresponding to the inner and outer radius is replaced with the corresponding line in **Dr1_3D**.

## B.2 Timestepping

Step two of the solver is the main step; here the matrix equations made in the previous step is timestepped using ODE15s.

### B.2.1 Initializing

ODE15s always need an inital condition for the temperature to start. The default choice of initial condition is the linear temperature distribution $T = (1 - z)$, but alternative intitial conditions can be given as input.

### B.2.2 Create Function for ODE15s to Solve

The timestepper ODE15s is only used to solve the energy equation (3.7), this being the only equation with a time derivative. ODE15s needs a (vector) function in the form $M\frac{dT}{dt} = f(T,t)$ to solve, where $T$ is now a vector in the form (B.1) and $M$ is the mass matrix. Using the differentiation matrices, we define $f$ to be a discrete version of

$$M\frac{dT}{dT} = \nabla^2 T - \mathbf{v}\cdot\nabla T,$$

where $\nabla^2$ and $\nabla$ are represented through differentiation matrices, and $\mathbf{v}$ is found using discrete versions of the Darcy equation (3.5) and the mass conservation equations (3.6) in each time step.

The mass matrix $M$ would normally be defined to be the identity matrix, but since we wish to remove the time derivatives in the matrix lines corresponding to boundary nodes, $M$ is the identity matrix with zeros on these lines. Hence, $M$ is singular and we therefore have a DAE-system. ODE15s and ODE23t are the only two of Matlab's ODE solvers capable of solving DAE-systems.

### B.2.3 Timestepping with ODE15s

Using the `options`() command in Matlab enables us to control the time stepping of ODE15s. We have used the `MaxStep` which controls the maximum step size, and `MaxOrder` which restricts the order of the adaptivity. The step size was restricted in order to prevent ODE15s to take too long time steps when the linear temperature $T = (1-z)$ was used as initial condition; this was because this temperature distribution also represents a possibly stable solution. In some cases we had to reduce the order of the solver to achieve better stability properties.

## B.3 Output

Even though ODE15s calculated the pressure and velocities in every time step, its only output is the temperature distribution. However, the pressures and velocities may be recalculated afterwards at required time steps using the now known temperature distribution. This way, the user may choose which output is wanted. In most simulations, we chose the temperature and velocity distribution for all time steps as output.

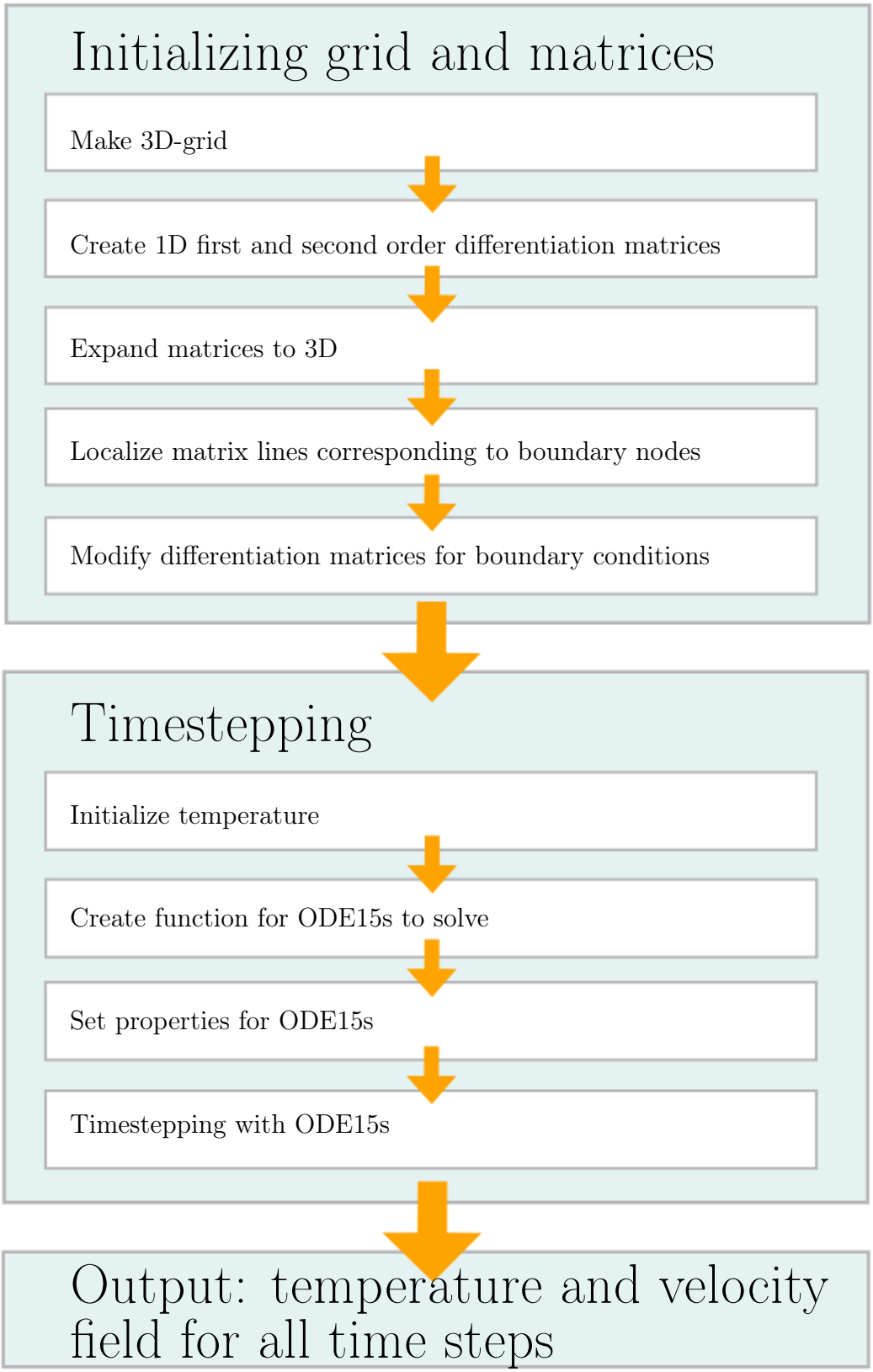




Figure B.1: Flow chart of simulator.

# Bibliography


[1] D. Bächler, T. Kohl, and L. Rybach. Impact of graben-parallel faults on hydrothermal convection–Rhine Graben case study. *Physics and Chemistry of the Earth, Parts A/B/C*, 28(9-11):431–441, 2003.

[2] H. H. Bau and K. E. Torrance. Onset of convection in a permeable medium between vertical coaxial cylinders. *Physics of Fluids*, 24(3):382–385, 1981.

[3] J. Bear. *Dynamics of fluids in porous media.* Dover Publications, 1988.

[4] J. L. Beck. Convection in a box of porous material saturated with fluid. *Physics of Fluids*, 15(8):1377–1383, 1972.

[5] A. Bejan and A. D. Kraus. *Heat Transfer handbook.* John Wiley and Sons, 2003.

[6] J. P. Boyd. *Chebyshev and Fourier spectral methods.* Dover Pubns, 2001.

[7] D. W. Brown. A hot dry rock geothermal energy concept utilizing supercritical CO2 instead of water. In *Proceedings, Twenty-Fifth Workshop on Geothermal Reservoir Engineering*, pages 233–238, 2000.

[8] D. S. Chapman and L. Rybach. Heat flow anomalies and their interpretation. *Journal of geodynamics*, 4(1-4):3–37, 1985.

[9] C. Clauser and H. Villinger. Analysis of conductive and convective heat transfer in a sedimentary basin, demonstrated for the Rheingraben. *Geophysical Journal International*, 100(3):393–414, 1990.

[10] N. Deichmann and D. Giardini. Earthquakes induced by the stimulation of an enhanced geothermal system below Basel (Switzerland). *Seismological Research Letters*, 80(5):784–798, 2009.

[11] D. Gottlieb, M. Y. Hussaini, and S. A. Orszag. Introduction: Theory and Applications of Spectral Methods. In R. G. Voigt, D. Gottlieb, and M. Y. Hussaini, editors, *Spectral Methods for Partial Differential Equations*. SIAM, 1984.

[12] D. Gottlieb and S. A. Orszag. *Numerical analysis of spectral methods: theory and applications*. Society for Industrial Mathematics, 1977.

[13] K. B. Haugen and P. A. Tyvand. Onset of thermal convection in a vertical porous cylinder with conducting wall. *Physics of Fluids*, 15(9):2661–2667, 2003.

[14] R. N. Horne and M. J. O'Sullivan. Convection in a porous medium heated from below: the effect of temperature dependent viscosity and thermal expansion coefficient. *Journal of Heat Transfer*, 100:448–452, 1978.

[15] C. W. Horton and F. T. Rogers. Convection currents in a porous medium. *Journal of Applied Physics*, 16(6):367–370, 2009.

[16] A. Kagel, D. Bates, and K. Gawell. *A guide to geothermal energy and the environment*. United States. Dept. of Energy. Geothermal Division, 2005.

[17] T. Kohl, D. Bächler, and L. Rybach. Steps towards a comprehensive thermo-hydraulic analysis of the HDR test site Soultz-sous-Forêts. In *Proceedings World Geothermal Congress*, pages 2671–2676, 2000.

[18] E. R. Lapwood. Convection of a fluid in a porous medium. In *Mathematical Proceedings of the Cambridge Philosophical Society*, volume 44, pages 508–521. Cambridge Univ Press, 1948.

[19] R. W. Lewis and K. N. Seetharamau. *Fundamentals of the Finite Element Method for Heat and Fluid Flow*. John Wiley and Sons, 2004.

[20] D. A. Nield. Onset of thermohaline convection in a porous medium. *Water Resources Research*, 4(3):553–560, 1968.

[21] D. A. Nield and A. Bejan. *Convection in Porous Media*. Springer, 3 edition, 2006.

[22] Ø. Pettersen. *Grunnkurs i RESERVOARMEKANIKK*. Matematisk institutt, Universitetet i Bergen, 1990.

[23] K. Pruess. Enhanced geothermal systems (EGS) using CO2 as working fluid–A novel approach for generating renewable energy with simultaneous sequestration of carbon. *Geothermics*, 35(4):351–367, 2006.

[24] K. Pruess. On production behavior of enhanced geothermal systems with CO2 as working fluid. *Energy Conversion and Management*, 49(6):1446–1454, 2008.

[25] D. A. S. Rees and P. A. Tyvand. The Helmholtz equation for convection in two-dimensional porous cavities with conducting boundaries. *Journal of engineering mathematics*, 49(2):181–193, 2004.

[26] M. W. Reichelt and L. F. Shampine. The matlab ode suite. *SIAM Journal on Scientific Computing*, 18(1):1–22, 1997.

[27] D. S. Riley and K. H. Winters. Modal exchange mechanisms in Lapwood convection. *Journal of Fluid Mechanics*, 204:325–358, 1989.

[28] J. W. Tester, B. Anderson, A. Batchelor, D. Blackwell, R. DiPippo, E. Drake, J. Garnish, B. Livesay, M. C. Moore, K. Nichols, et al. The future of geothermal energy: impact of Enhanced Geothermal Systems (EGS) on the United States in the 21st Century. *Final Report to the US Department of Energy Geothermal Technologies Program. Cambridge, MA.: Massachusetts Institute of Technology*, 2006.

[29] L. N. Trefethen. *Spectral methods in MATLAB*. Society for Industrial Mathematics, 2000.

[30] K. Vafai. Convective flow and heat transfer in variable-porosity media. *Journal of Fluid Mechanics*, 147:233–259, 1984.

[31] C. Y. Wang. Onset of convection in a fluid-saturated rectangular box, bottom heated by constant flux. *Physics of Fluids*, 11(6):1673–1675, 1999.

[32] C. Y. Wang. Thermo-convective stability of a fluid-saturated porous medium inside a cylindrical enclosure: Permeable top constant flux heating. *Mechanics research communications*, 26(5):603–608, 1999.

[33] A. Zebib. Onset of natural convection in a cylinder of water saturated porous media. *Physics of Fluids*, 21(4):699–700, 1978.